The Pennsylvania State University

The Graduate School

Department of Chemistry

SUBSTRATE POSITIONING AND CHANNELING OF ESCHERICHIA COLI QUINOLINATE SYNTHASE

A Thesis in

Chemistry

by

Lauren A. Sites

Submitted in Partial Fulfillment
of the Requirements
for the Degree of

Master of Science

December 2012

The thesis of Lauren A. Sites was reviewed and approved* by the following:

Squire J. Booker
Associate Professor of Chemistry
Thesis Advisor

Carsten Krebs
Professor of Chemistry

Scott A. Showalter
Assistant Professor of Chemistry

Kenneth S. Feldman
Professor of Chemistry
Head of Department

*Signatures are on file in the Graduate School

ABSTRACT

The essential cofactor nicotinamide adenine dinucleotide (NAD) is consumed in many metabolic reactions in the cell, necessitating the need to synthesize NAD. In most bacteria, the *de novo* pathway to form NAD begins with two unique enzymes that have been extensively studied herein. The first enzyme in the pathway, L-aspartate oxidase, performs a two-electron oxidation of L-aspartate to form iminoaspartate. This flavin containing enzyme can undergo multiple catalytic turnovers given the oxidants, fumarate or molecular oxygen, to afford the oxidized form of the enzyme. The second enzyme in the pathway, quinolinate synthase or NadA, condenses iminoaspartate and dihydroxyacetone phosphate to form quinolinic acid, the backbone of the pyridine ring of NAD.

Many have postulated that these two enzymes can operate as an enzyme complex, yet no substantial evidence of this complex has been demonstrated. Investigations to examine the possible protein-protein interactions of the two enzymes were carried out, yet no obvious interaction was seen by the techniques employed. The oxygen-sensitive nature of Fe/S cluster of NadA and the kinetics of NadB prevented gathering data to conclude a concrete finding.

The mechanism of NadA is still unknown despite discovering its requirement for a [4Fe-4S] cluster for activity over seven years ago. While it was speculated and now shown by others, that the Fe/S cluster acts a Lewis acid to aid in the final dehydration of a reaction intermediate to form quinolinic acid, no evidence exists with native substrates coordinating to the Fe/S cluster. The advanced spectroscopic techniques, EPR and ENDOR, were employed to examine NadA with various substrates. While it is known what carbon of DHAP is closest to the Fe/S cluster, an ENDOR signal was not seen when NadA was incubated with ^{13}C-labeled DHAP.

TABLE OF CONTENTS

LIST OF ABBREVIATIONS

anSME	anaerobic sulfatase maturating enzyme
anSMEcpe	anaerobic sulfatase maturating enzyme from *Clostridium perfringens*
AI	as-isolated
ADP	adenosine dephosphate
AMP	adenosine monophosphate
ATP	adenosine triphosphate
DHAP	dihydroxyacetone phosphate
DTT	dithiothreitol
Ec	*Escherichia coli*
EDTA	ethylenediaminetetraacetic acid
ENDOR	electron nuclear double resonance
EPR	electron paramagnetic resonance
ES	external standard
FAD	flavin adenine dinucleotide
FDR	fumarate reductase
Fe/S	iron sulfur
G-3-P	glyceraldehyde-3-phosphate
HEPES	*N*-(2-hydroxyethyl)piperizine-*N*'-(2-ethanesulfonic acid)
HPLC	high-performance liquid chromatography
IA	iminoaspartate
IMAC	immobilized metal affinity chromatography
IPTG	isopropyl-β-D-thiogalactopyranoside

IS	internal standard
ITC	isothermal calorimetry
KIE	kinetic isotope effect
LB	Luria-Bertani
LC-MS	liquid chromatography-mass spectroscopy
Mtb	*Mycobacterium tuberculosis*
NAD	nicotinamide adenine dinucleotide
NadA	quinolinate synthase
$NadA_{ox}$	oxidized quinolinate synthase
$NadA_{red}$	reduced quinolinate synthase
NadB	L-aspartate oxidase
NADP	nicotinamide adenine dinucleotide phosphate
Ni-NTA	nickel nitrilotriacetic acid
NMR	nuclear resonance spectroscopy
OAA	oxaloacetate
Pi	inorganic phosphate
PCR	polymerase chain reaction
PDA	photodiode array
Ph	*Pyrococcus horikoshii*
PMSF	phenylmethanesulfonyl floride
PMT	photomultiplier tube
QA	quinolinic acid
RCN	reconstituted
SAH	*S*-adenosylhomocysteine

SDH	succinate dehydrogenase
SDS-PAGE	sodium dodecylsulfate-polyacrylamide gel electrophoresis
TCA	trichloroacetic acid
TFA	trifluoroacetic acid
TIM	triosephosphate isomerase
Tris	tris(hydroxymethyl)aminomethane
Trx	thioredoxin
Trx_{ox}	oxidized thioredoxin
Trx_{red}	reduced thioredoxin
WT	wild-type

LIST OF FIGURES

.

LIST OF TABLES

ACKNOWLEDGEMENTS

I would like to thank all those who have inspired, taught, and encouraged me to be the best I can be. I am a product of my environment and therefore have been successful because of you.

Chapter 1

NAD Biosynthesis in Bacteria

Nicotinamide adenine dinucleotide (NAD) and its reduced and phosphorylated forms are utilized in hundreds of oxidation-reduction reactions in the cell. In these reactions, a two-electron hydride transfer occurs at C-4 of the nicotinamide ring (Figure 1-1). This essential metabolite also participates in a number of non-redox reactions in the cell where it is used as a substrate and has been shown to impact cellular processes including cell signaling, Ca^{2+} mobilization, and apoptosis (*1*).

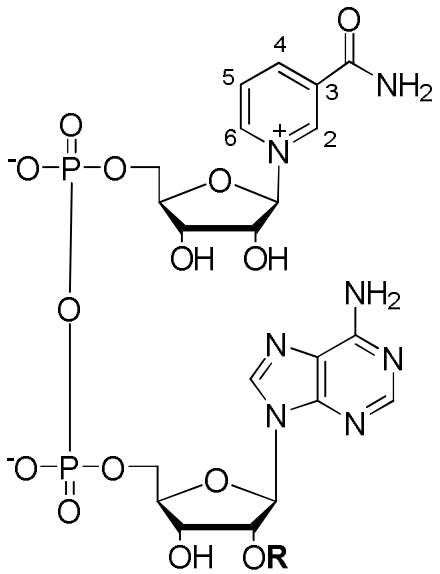

Figure **1-1**: Structure of NAD(P). NAD: R = H, NADP: R = Phosphate (HPO_3).

1.1 NAD metabolism

Though NAD in oxidation-reduction reactions is well studied, the discovery of enzymes that consume NAD and their wide variety of reaction types has been noteworthy. One class of NAD-dependent enzymes sirtuins, are enzymes that affect multiple cellular processes including stress responses, inflammation, and protein aggregation (*2*). Sirtuins remove the acetyl group from acetyllysine-modified proteins and have the ability to target a wide variety of enzymes including the N-terminal tail of histones and transcription factors (*3*). These enzymes transfer the targeted acetyl group to the 2′ -position of the ribose ring of NAD. This step facilitates loss of the nicotinamide moiety of NAD. The free nicotinamide is thought to feed back into the salvage/recycling NAD pathway to support NAD biosynthesis (see Section 1.3).

Poly(ADP-ribose) polymerases (PARP) are enzymes that are activated by DNA strand breakage and play an important role in the organization of the repair of damaged DNA. These enzymes break the N′-glycosidic bond of NAD and transfer the ADP-ribose moiety to a glutamate residue on a target protein (Figure 1-2) (*3*). Analogous to sirtuins, the released nicotinamide is thought to proceed in the recycling pathway to form NAD. While this type of activation is signaled upon DNA damage, PARPs can actually deplete the cellular pool of NAD and cause premature cell death. Small molecule inhibitors of PARPs are thought to promote cell longevity (*3*).

In bacteria, a double-stranded DNA break can be repaired by the action of DNA ligase. This enzyme uses an active site lysine to split the phosphodiester bond of NAD and form an enzyme-adenylated intermediate (Figure 1-2) (*4*). The AMP intermediate is transferred to the 5′ end of the DNA nick to form a DNA-adenylate intermediate. Attack of the free hydroxyl of the 3′ strand of DNA releases AMP and re-ligates the strand of DNA. The other product of this reaction is nicotinamide mononucleotide (NMN) (*5*). This mechanism is essentially the same in

higher organisms; the reaction uses the same intermediates though ATP is used instead of NAD. This enzyme is an interesting target for drugs that could selectively inhibit bacterial DNA ligases.

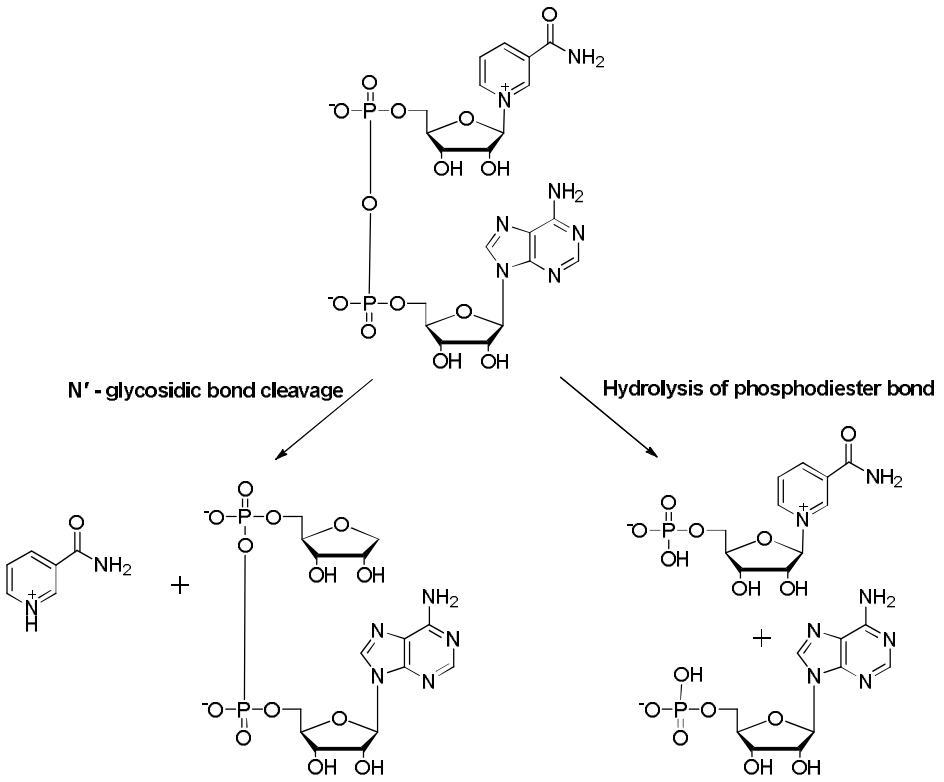

Figure **1-2**: Common products of non-redox NAD-dependent enzymes. N′ -glycosidic bond cleavage of NAD performed by sirtuins and PARPS, while DNA ligase cleaves NAD at the phosphodiester bond to produce two nucleotides.

Because NAD is a metabolite that is consumed and constantly needs to be regenerated, the biosynthesis of NAD is tightly regulated. Though NAD can be expended such as in the previously discussed reactions, levels of all forms of the dinucleotide are regulated and subject to changes upon stress or other environmental stimuli. In an oxidative environment, the levels of reactive oxygen species (ROS) and other oxidants can be combated by the reducing power of NADH. Oxygen exposure also increases production of NAD, while NADH levels remain the

same. Consequently, NAD is consumed at a greater rate under aerobic conditions than under anaerobic conditions (*6*).

In nearly every organism, there is a *de novo* pathway in which NAD is synthesized from precursor metabolites. This pathway to form NAD differs between prokaryotes and eukaryotes, yet both pathways share the intermediate QA. The enzymes, later in the pathway, supporting NAD production from QA are then homologous. Most eukaryotes begin the *de novo* pathway with L-tryptophan, while most prokaryotes and some plants use L-aspartate and dihydroxyacetone phosphate to form the pyridine ring of QA. Since there are remarkable differences in the pathways to form QA in prokaryotes and eukaryotes, the prokaryotic pathway was thought to provide a target for antibacterial drugs (*4*).

1.2 *de novo* NAD biosynthesis in bacteria

L-aspartate oxidase

The first enzyme of the prokaryotic *de novo* pathway was characterized by Gholson and coworkers (*7*). L-aspartate oxidase or NadB uses a non-covalently bound FAD molecule to oxidize L-aspartate to iminoaspartate (IA) (Figure 1-3). To regenerate the FAD, molecular oxygen or fumarate can act as an oxidizing agent affording hydrogen peroxide or succinate, respectively (*8*). The product of the NadB reaction, IA, is unstable and noted to have a half-life of 150 s at pH 8.0 at 25°C, as IA can readily undergo hydrolysis and/or β-decarboxylation to form OAA or pyruvate (*9*). Binding studies show that NadB binds IA very tightly with a K_D of 1.4 μM (*8*). Anaerobic turnover of the enzyme proceeds through a ping-pong mechanism where fumarate and IA compete for the same binding site. Under oxic conditions, a ternary complex with O_2 is formed before IA is released (*8*).

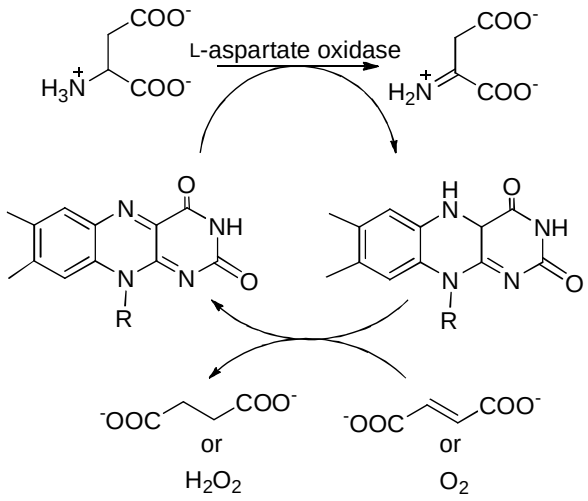

Figure **1-3**: Action of the enzyme L-aspartate oxidase. R = D-ribitol-ADP

The majority of the mechanistic focus of NadB has utilized crystal structures to note the differences between NadB and flavin-containing fumarate reductases/succinate dehydrogenases where fumarate reduction is much faster (*10*, *11*). NadB is composed of three domains: a FAD binding domain, a capping domain, and a helical domain with the active site located in a large cleft between the FAD-binding and capping domains (*10*). NadB uses an α-β dehydrogenation mechanism to oxidize L-aspartate, where an active site arginine (R290 in *E. coli*) abstracts a proton from C2 of L-aspartate and a hydride from C3 is transferred to FAD (Figure 1-4) (*11*). NadB is a weak fumarate reductase due to the fact that the same active site must accommodate both fumarate as well as L-aspartate, which is an asymmetric molecule (*13*). To compensate for the asymmetry, the active site of NadB contains a conserved glutamate (Glu121 in *E. coli*) which stabilizes the α-amino group of L-aspartate, while other fumarate reductases contain an aliphatic amino acid at the position (*11*).

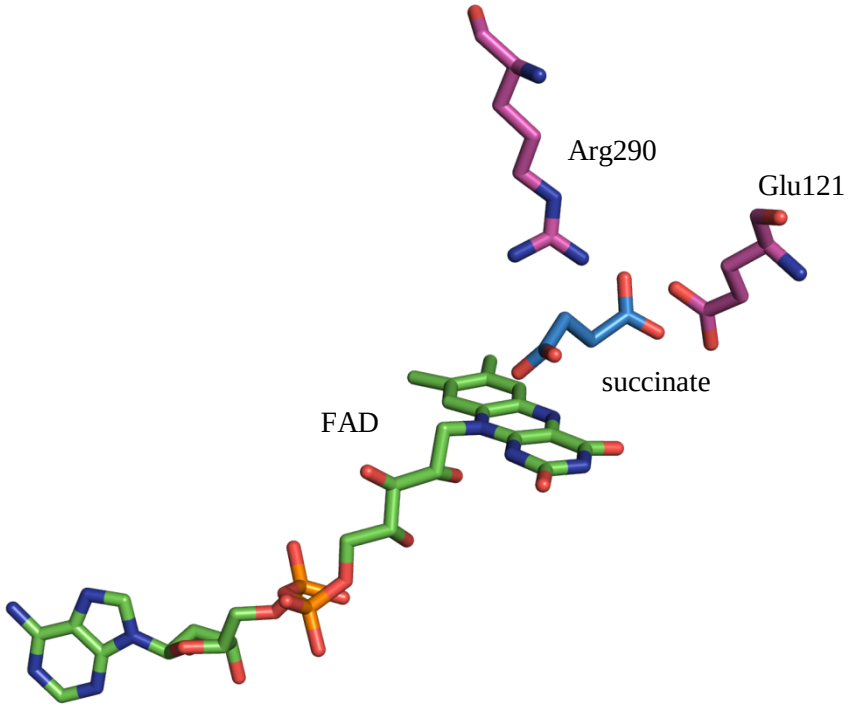

Figure **1-4**: Crystal structure of L-aspartate oxidase R386L with FAD and succinate.

Quinolinate Synthase

The other enzyme unique to the prokaryotic pathway in NAD biosynthesis is quinolinate synthase or NadA. This enzyme condenses IA with DHAP to form QA (Figure 1-5). The enzyme was noted to be highly labile and was not recovered in high enough yield to be studied directly in early studies (*14*). In general studies monitoring NAD biosynthesis, NadA was noted to be the step of "oxygen poisoning" (*15*). In 1991, it was proposed that the enzyme's oxygen sensitivity may be due to the presence of a Fe/S cluster (*16*). Nearly ten years later, a publication cited the successful aerobic purification of *E. coli* NadA where protein was purified from inclusion bodies (*17*). Though assays were carried out aerobically and anaerobically, the protein

was isolated in a buffer containing EDTA in an aerobic environment thus ensuring no Fe/S cluster could be bound.

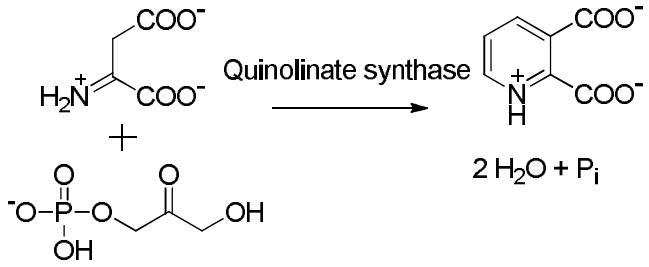

Figure **1-5**: Reaction catalyzed by quinolinate synthase (NadA).

Conversely in 2005, two laboratories showed that NadA does contain a [4Fe-4S] cluster by quantitative iron and sulfide content, spectroscopic methods, and activity assays, and that the cluster is required for catalysis (*18*, *19*). The role of the Fe/S cluster was not clear upon initial inspection, yet it was thought to function as a Lewis acid to assist in a dehydration like other enzymes in the Fe/S-dependent hydrolyase class, such as aconitase (*18*, *19*). Gholson and coworkers proposed a mechanism for NadA, after performing radioactivity labeling studies of DHAP to confirm which carbons of the reactants transformed to carbons of the product (*7*, *20*). His mechanism involves an S_N2-type direct attack onto C1 of DHAP by the enamine form of IA to release inorganic phosphate (P_i) (Figure 1-6). Abstraction of a proton from C3 of DHAP forms an ene-diol intermediate. Tautomerization creates an aldehyde, which the neutral amine can attack to form the six-membered ring of quinolinic acid. The last two steps, the elimination of two water molecules, create the aromaticity in the pyridine ring of QA. While this mechanism does not directly account for the Fe/S cluster, one can postulate that the Fe/S cluster of NadA acts as a Lewis acid to aid in the final dehydration step.

Another mechanism was proposed by Begley in which DHAP tautomerizes to the intermediate G-3-P (Figure 1-6) (*21*). In this mechanism, the enamine form of IA forms a Schiff's base with G-3-P as the initial step. Tautomerization of the aldehyde to a primary enol then promotes electrocyclic ring closure. As with the previous mechanism, the elimination of water is proposed to be carried out with the aid of the Fe/S cluster. Though early studies supported the premise that NadA could use G-3-P as a substrate, it was suspected that triosephopshate isomerase (TIM) contamination could easily convert the G-3-P to DHAP (*14*).

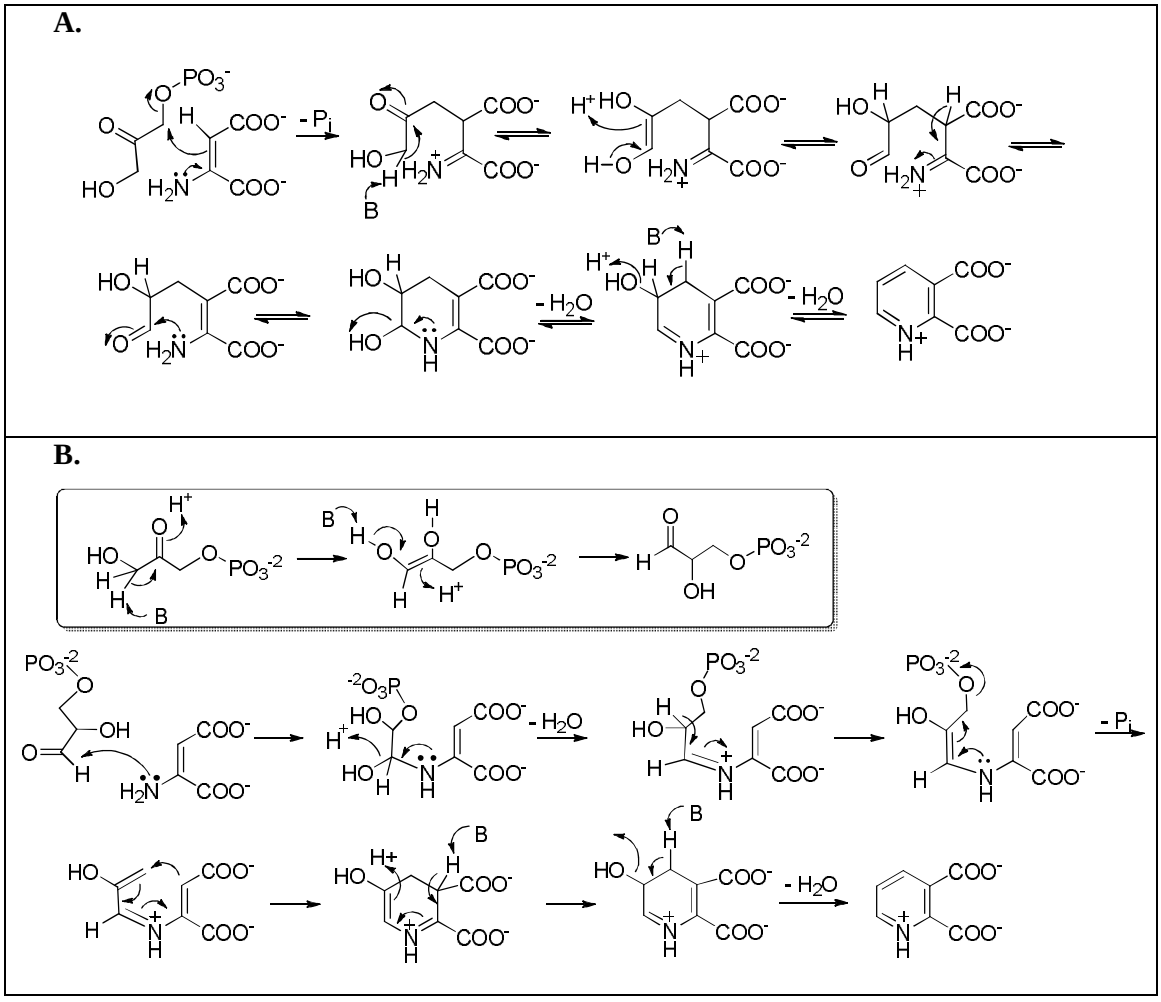

Figure **1-6**: Mechanisms proposed by Gholson (*7*) (Panel A) and Begley (*21*) (Panel B).

Though these two mechanisms differ considerably, they share the same final step, a dehydration facilitated by the Fe/S cluster. This type of reaction, where the Fe/S cluster aids in dehydration, is analogous to the role of the [4Fe-4S] cluster in aconitase. A member of the hydrolyase class of enzymes, aconitase converts citrate to isocitrate using a [4Fe-4S] cluster as a Lewis acid (*22*). The enzyme coordinates a [4Fe-4S] through 3 conserved cysteine residues and the open iron site coordinates the carboxyl and hydroxyl groups of the substrate (*23*). The Fe/S cluster aids in the removal of the hydroxyl group from citrate, to form the cis-aconitate intermediate, then rebounds the hydroxyl group after the intermediate is released to change its conformation. Evidence that the Fe/S cluster of NadA can function as a Lewis acid was recently provided by Chan *et al.*, where dithiohydroxyphthalic acid (DTHPA) served as a potent inhibitor of the reaction. Mössbauer spectroscopy and density functional theory (DFT) analysis of the NadA/DTHPA complex showed evidence of a unique iron that was bound in a bidentate fashion to the thiol groups at C5 and C6 of DTHPA (*24*).

At the same time NadA was shown to contain a [4Fe-4S] cluster, Sakuraba *et al*. solved a crystal structure of *Pyrococcus horikoshii* NadA with malate − a substrate analog of IA − bound in the active site (Figure 1-7) (*25*). The structure shows three domains with triangular symmetry each having an αβα sandwich fold. The electron density of the loops connecting each domain was not resolved. Malate was bound in the center of the protein, and surrounded by amino acids that are conserved among all quinolinate synthases, suggesting the location of the active site. The other substrate, DHAP, could not be modeled into the active site, because its phosphate group could not be sterically accommodated. In addition, the tertiary complex containing DHAP and IA could not be crystallized by soaking the malate-bound NadA crystals with DHAP (*25*).

Figure **1-7**: Quinolinate synthase crystal structure containing malate (gold). Adapted from Sakuraba *et al.*

While portions of the structure were poorly resolved, there was no mention of the possibility of an Fe/S cluster. Further, the activity the authors reported for the enzyme lacking the Fe/S cluster was over ten times higher than that reported by Cicchillo *et al*. for the *E. coli* enzyme containing a [4Fe-4S] cluster (*19*). While the crystal structure provided tertiary and quaternary structural information, the unresolved portions of the active site limited detailed mechanistic analysis.

The [4Fe-4S] cluster of NadA was shown to be ligated by three conserved cysteine residues by a series of site-directed mutagenesis experiments coupled with analysis for iron and sulfide, activity determinations, and spectroscopic characterization of the variant proteins (*26*, *27*). Upon examination of the primary structure of NadA, *E. coli* NadA was noted to have a **C**XX**C**XX**C** motif, which is similar to that of ferredoxin-like enzymes (*28*). This sequence, however, was not conserved among all quinolinate synthases and only one cysteine in this motif was shown to be a cluster ligand. Site-directed mutagenesis was also performed with *P. horikoshii* NadA (*26*). The cysteines ligating the Fe/S cluster in the enzyme are found in the

loops that were unable to be resolved in the 2005 *Pyrococcus horikoshii* NadA crystal structure. It is conceivable that the presence of the Fe/S cluster would stabilize the loops containing the cysteines to allow the electron density to be solved.

The remaining cysteines in the motif form a disulfide bond under oxidizing conditions (*27*, *29*). Thioredoxin (Trx), a disulfide oxidoreductase that maintains the reduced environment in the cytosol, was capable of reducing the *E. coli* NadA disulfide bond. Using a titration of reduced to oxidized Trx, where Trx has a redox potential of -271 mV (*30*), the *E. coli* NadA disulfide bond was found to have a redox potential of -264 mV (*29*). The presence of the disulfide bond increased activity of NadA, yet the role of this activation is unknown and seemed to suggest some type of oxidative regulation occurs *in vivo* to control QA production.

The remaining steps in pathway

Once QA is formed by NadA, quinolinic acid phosphoribosyl transferase, or NadC, forms nicotinic acid mononucleotide (NaMN) (Figure 1-8) (*31*). While the pyridine nucleotide pathway utilizes a number of phosphoribosyl transferases, each enzyme is specific for its particular substrate, in this case QA. NadC performs a decarboxylation while using 5-phosphoribosyl-1-pyrophosphate (PRPP) to form a nucleotide (*32*). The reaction yields nicotinic acid mononucleotide (NaMN), pyrophosphate (PP_i) and CO_2. This enzyme is critical in the removal of QA which is toxic in eukaryotes at high concentrations (*4*). NaMN is acted upon by NaMN adenyl transferase or NadD to insert the second nucleotide of NAD, wherein ATP is used to append AMP to NaMN. The last step in the pathway to form NAD is amidation of the nicotinic acid moiety of NaAD. The amine source can come from ammonia or glutamate depending on the organism and requires hydrolysis of one ATP molecule (*32*). To form the phosphorylated forms of NAD, NAD kinase transfers a phosphate group to the adenosyl ribose. The levels of NAD/NADP are highly regulated and under starvation conditions, NAD levels are sacrificed to

maintain NADP levels (*32*). NAD kinase is regulated by Ca^{2+}-calmodulin, an important messenger protein in the cell (*4*).

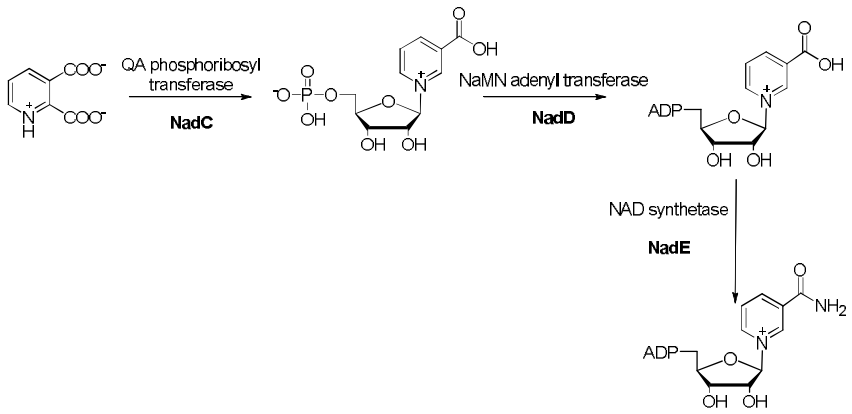

Figure **1-8**: Biosynthesis of NAD from the intermediate QA.

Regulation of the *de novo* pathway is primarily performed by NadR, a transcriptional repressor of *nadB* and *nadA* (*33*). Acting as a dimer, NadR can bind to a consensus sequence of DNA called the NAD box. This enzyme also senses levels of NAD in the cell via a NAD-binding domain (*34*). NadR also controls expression of nicotinic acid phosphoribosyl transferase and facilitates transport of nicotinamide adenine mononucleotide into the cell, though the mechanism of these actions is not well understood (*34*). In addition to regulation by NadR, NadB shows feedback inhibition by NAD and its reduced and phosphorylated forms (*35*).

1.3 Recycling and Salvage Pathways

While nearly all organisms contain a *de novo* pathway to form NAD, most organisms can utilize breakdown products of NAD to synthesize the essential cofactor/substrate. These pathways, known as recycling or salvage pathways, were illuminated in studies wherein knockouts of some of the genes in the NAD operon could be rescued by nicotinic acid or

nicotinamide (*36*). While these molecules are not substrates in the *de novo* pathway, they support an alternative pathway to supply the cell with NAD (*33*). These pathways are energetically more favorable than the *de novo* pathway and are utilized when nicotinic acid or nicotinamide are available (*37*). Some organisms, such as *Candida glabrata* and *Haemophilus influenza,* lack a *de novo* pathway and depend solely on the scavenging of pyridine precursors to synthesize NAD (*38*). *Mycobacterium tuberculosis* was once thought to have a nonfunctioning salvage pathway, yet has recently been shown to be able obtain nicotinamide from its host (*39*).

Nicotinamide is the byproduct of many reactions discussed previously (see Section 1.1). One way for nicotinamide to be used in NAD biosynthesis is to undergo deamination to form nicotinic acid (Figure 1-9). Nicotinic acid is the preferred salvage product in *E. coli* and can enter the *de novo* pathway by nicotinic acid phosphoribosyl transferase, which forms nicotinic acid mononucleotide (NaMN). Nicotinamide phosphoribosyl transferase can convert nicotinamide to nicotinamide mononucleotide (NMN); however, this enzyme is the rate-limiting step from nicotinamide to NAD and is induced by cell stress and nutrient restriction (*4*). NMN, a product from the reaction catalyzed by DNA ligase, can enter the *de novo* pathway by NMN adenyltransferase, which adds the second nucleotide moiety to the molecule, or via NMN deamidase which forms NaMN.

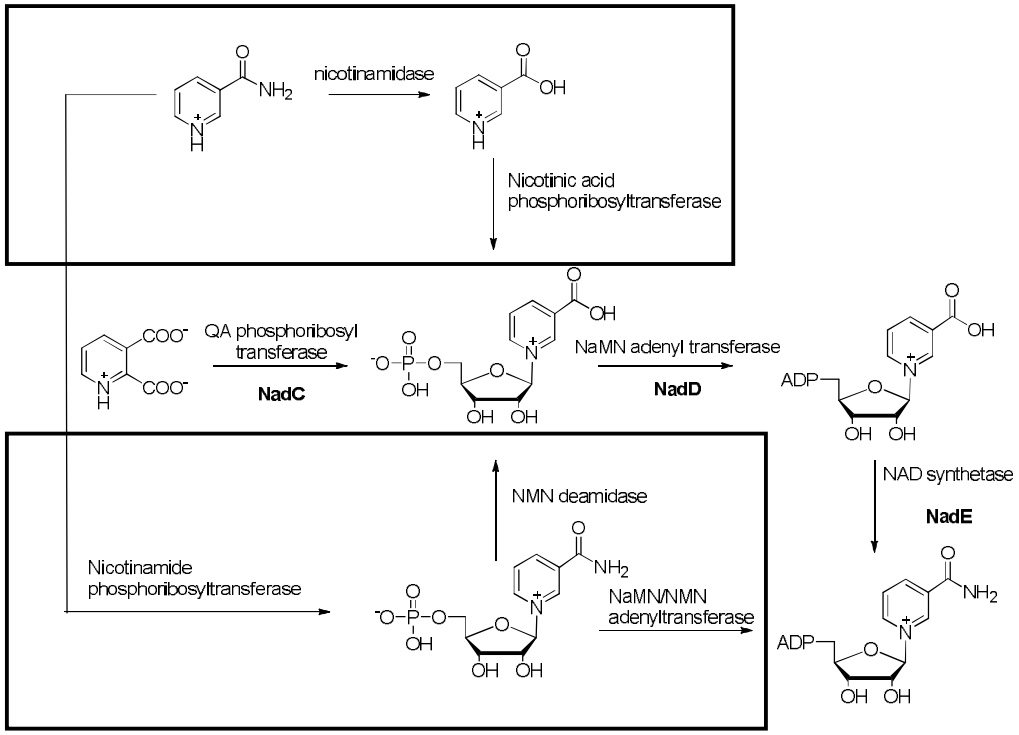

Figure **1-9**: Recycling and salvage pathways for NAD biosynthesis (highlighted in boxes).

1.4 Discussion

NAD, as a redox cofactor and a substrate for many biological reactions, is an indispensible metabolite in the cell. Though studies of the *de novo* pathway have been ongoing since the 1950's, many of the enzymes in the pathway have been only recently characterized. Enzymes that are present in pathogenic bacteria and not in the eukaryotic host are of particular interest for the development of novel antibiotics. Until recently, evidence suggested that *Mycobacterium tuberculosis* had a non-functioning salvage pathway and efforts to inhibit *de novo* NAD biosynthesis would yield a successful drug target (*40*). More recent studies show that *M. tuberculosis* is in fact able to obtain intermediates in the salvage pathway from their host organism (*39*). Recent bioinformatic studies show *Helicobacter pylori* and *Mycobacterium*

leprae, lack a salvage pathway and that inhibiting the *de novo* pathway unique to prokaryotes might still be a fruitful antibacterial agent (*39*). Plants, which use the same *de novo* pathway as most bacteria, also have been studied to better understand the biosynthesis of NAD. In a mutant strain of *Arabidoposis thaliana* where the *nadA* gene was nonfunctioning, the plant compensated by utilizing only the salvage pathway to synthesize NAD and the other pyridine nucleotide cofactors. This strain displayed unusually high reactive oxygen species (ROS) which may be related to the up-regulation of NadB (*41*). Though the enzymatic steps of the *de novo* and salvage pathways are known, regulation and *in vivo* control of NAD biosynthesis is clearly more complex than originally thought.

Many mechanistic questions regarding the first two enzymes in the *de novo* pathway have yet to be solved. While NadB has been characterized in greater detail, mechanistically and structurally, it seems contradictory for an oxygen-utilizing enzyme to precede an oxygen labile enzyme in the pathway. With the evidence that *E.coli* NadA is redox-regulated by disulfide bond formation, it suggests the pathway is regulated by some type of redox mechanism. Further, it has been hypothesized that NadB and NadA act in concert or as a complex were originally purposed, yet data to support this claim is lacking (*42*).

While it has been shown indisputably that NadA contains a Fe/S cluster that is required for catalysis, many questions still remain regarding the NadA mechanism. Attempts to resolve the role of the Fe/S cluster of NadA were carried out prior to the Chan *et al*. publication where spectroscopic evidence supports the role of the unique iron site binding the C5 substituent of the pyridine ring (*24*). Though the role of the Fe/S cluster of NadA confirms its place in the hydrolyase class of enzymes, the complete mechanism of NadA is still unresolved.

1.5 References

(1) Bogan, K. L.; Brenner, C. Nicotinic acid, nicotinamide, and nicotinamide riboside: a molecular evaluation of NAD^+ precursor vitamins in human nutrition. *Annual review of nutrition* **2008**, *28*, 115–130.

(2) Donmez, G. The neurobiology of sirtuins and their role in neurodegeneration. *Trends in pharmacological sciences* **2012**, 1–8.

(3) Yang, T.; Sauve, A. NAD metabolism and sirtuins: metabolic regulation of protein deacetylation in stress and toxicity. *The AAPS journal* **2006**, *8*, 632–643.

(4) Magni, G.; Amici, A.; Emanuelli, M.; Raffaelli, N. Enzymology of NAD^+ Biosynthesis. In *Advances in Enzymology and Related Areas of Molecular Biology, Volume 73*; 1999; pp. 135–182.

(5) Doherty, A. J.; Suh, S. W. Structural and mechanistic conservation in DNA ligases. *Nucleic Acids Research* **2000**, *28*, 4051–4058.

(6) Wimpenny, J. W.; Firth, A. Levels of nicotinamide adenine dinucleotide and reduced nicotinamide adenine dinucleotide in facultative bacteria and the effect of oxygen. *Journal of bacteriology* **1972**, *111*, 24–32.

(7) Nasu, S.; Wicks, D.; Gholson, R. K. L-Aspartate Oxidase, a Newly Discovered Enzyme of *Escherichia coli*, Is the B protein of Quinolinate Synthetase. *J. Biol. Chem.* **1982**, *257*, 626–632.

(8) Tedeschi, G.; Negri, A.; Mortarino, M.; Ceciliani, F.; Simonic, T. L-Aspartate oxidase from *Escherichia coli* II. Interaction with C4 dicarboxylic acids and identification of a novel L-aspartate:fumarate oxidoreductase activity. *European Journal of Biochemistry* **1996**, *433*, 427–433.

(9) Nasu, S.; Gholson, R. K. Replacement of the B protein Requirement of the *E. coli* Quinolinate Synthetase System by Chemically-Generated Iminoaspartate. *Biochemical and Biophysical Research Communications* **1981**, *101*, 533–539.

(10) Mattevi, A.; Tedeschi, G.; Bacchella, L.; Coda, A.; Negri, A.; Ronchi, S. Structure of L-aspartate oxidase: implications for the succinate dehydrogenase/fumarate reductase oxidoreductase family. *Structure (London, England : 1993)* **1999**, *7*, 745–756.

(11) Tedeschi, G.; Nonnis, S.; Strumbo, B.; Cruciani, G.; Carosati, E.; Negri, A. On the catalytic role of the active site residue E121 of *E. coli* L-aspartate oxidase. *Biochimie* **2010**, *92*, 1335–42.

(12) Tedeschi, G.; Negri, A.; Ceciliani, F.; Mattevi, A.; Ronchi, S. Structural characterization of L-aspartate oxidase and identification of an interdomain loop by limited proteolysis. *European journal of biochemistry / FEBS* **1999**, *260*, 896–903.

(13) Bossi, R. T.; Negri, A.; Tedeschi, G.; Mattevi, A. Structure of FAD-bound L-aspartate oxidase: insight into substrate specificity and catalysis. *Biochemistry* **2002**, *41*, 3018–3024.

(14) Chandler, J. L., Gholson, R. K. Studies on the Biosynthesis of NAD in *Escherichia coli* iii. Precursors of Quinolinic Acid *in vitro*. *Biochemica and Biophysica Acta* **1971**, *264*, 311–318.

(15) Dracyznska-Lusiak, B.; Brown, O. R. Protein A of quinolinate synthetase is the site of oxygen poisoning of pyridine nucleotide coenzyme synthesis in *Escherichia coli*. *Free Rad Biol Med* **1992**, *13*, 689–693.

(16) Gardner, P. R.; Fridovich, I. Quinolinate synthetase: the oxygen-sensitive site of *de novo* $NAD(P)^+$ biosynthesis. *Archives of biochemistry and biophysics* **1991**, *284*, 106–111.

(17) Ceciliani, F.; Caramori, T.; Ronchi, S.; Tedeschi, G.; Mortarino, M.; Galizzi, A. Cloning, overexpression, and purification of *Escherichia coli* quinolinate synthetase. *Protein expression and purification* **2000**, *18*, 64–70.

(18) Ollagnier-de Choudens, S.; Loiseau, L.; Sanakis, Y.; Barras, F.; Fontecave, M. Quinolinate synthetase, an iron-sulfur enzyme in NAD biosynthesis. *FEBS letters* **2005**, *579*, 3737–3743.

(19) Cicchillo, R. M.; Tu, L.; Stromberg, J. A.; Hoffart, L. M.; Krebs, C.; Booker, S. J. *Escherichia coli* quinolinate synthetase does indeed harbor a [4Fe-4S] cluster. *Journal of the American Chemical Society* **2005**, *127*, 7310–7311.

(20) Wicks, F. D.; Sakakibara, S.; Gholson, R. K.; Scott, T. A. The Mode of Condensation of Aspartic acid and Dihydroxyacetone Phosphate in Quinolinate Synthesis in *Escherichia coli*. *Biochimica et biophysica acta* **1977**, *500*, 213–216.

(21) Begley, Tadhg P., Kinsland, Cynthia, Mehl, R. A., Osterman A., Dorrestein, P. The biosynthesis of nicotinamide adenine dinucleotides in bacteria. In *Vitamins & Hormones*; 2001; pp. 103–119.

(22) Flint, D. H.; Allen, R. M. Iron-Sulfur Proteins with Nonredox Functions. *Chemical Reviews* **1996**, *7*, 2315–2334.

(23) Kennedy, M. C.; Werst, M.; Telser, J.; Emptage, M. H.; Beinert, H.; Hoffman, B. M. Mode of substrate carboxyl binding to the $[4Fe\text{-}4S]^{+}$ cluster of reduced aconitase as studied by ^{17}O and ^{13}C electron-nuclear double resonance spectroscopy. *Proceedings of the National Academy of Sciences of the United States of America* **1987**, *84*, 8854–8858.

(24) Chan, A.; Clémancey, M.; Mouesca, J.-M.; Amara, P.; Hamelin, O.; Latour, J.-M.; Ollagnier de Choudens, S. Studies of Inhibitor Binding to the [4Fe-4S] Cluster of Quinolinate Synthase. *Angewandte Chemie* **2012**, *124*, 7831–7834.

(25) Sakuraba, H.; Tsuge, H.; Yoneda, K.; Katunuma, N.; Ohshima, T. Crystal structure of the NAD biosynthetic enzyme quinolinate synthase. *The Journal of biological chemistry* **2005**, *280*, 26645–26648.

(26) Saunders, A. H.; Griffiths, A. E.; Lee, K.-H.; Cicchillo, R. M.; Tu, L.; Stromberg, J. A.; Krebs, C.; Booker, S. J. Characterization of quinolinate synthases from *Escherichia coli*, *Mycobacterium tuberculosis*, and *Pyrococcus horikoshii* indicates that [4Fe-4S] clusters are common cofactors throughout this class of enzymes. *Biochemistry* **2008**, *47*, 10999–11012.

(27) Rousset, C.; Fontecave, M.; Ollagnier de Choudens, S. The [4Fe-4S] cluster of quinolinate synthase from *Escherichia co*li: investigation of cluster ligands. *FEBS letters* **2008**, *582*, 2937–2944.

(28) Bruschi, M.; Guerlesquin, F. Structure, function and evolution of bacterial ferredoxins. *FEBS Microbiol. Rev.* **1988**, *4*, 155–175.

(29) Saunders, A. H.; Booker, S. J. Regulation of the Activity of *Escherichia coli* Quinolinate Synthase by Reversible Disulfide-Bond Formation. *Biochemistry* **2008**, *47*, 8467–8469.

(30) Krauses, G.; Lundstrom, J.; Bareas, J. L.; De, C. P.; Holmgrenii, A. Mimicking the Active Site of Protein Disulfide-Isomerase by Substitution of Proline 34 in *Escherichia coli* Thioredoxin. *The Journal of biological chemistry* **1991**, *266*, 9494–9500.

(31) Sharma, V.; Grubmeyer, C.; Sacchettini, J. C. Crystal structure of quinolinic acid phosphoribosyltransferase from *Mycobacterium tuberculosis* : a potential TB drug target. *Structure* **1998**, *6*, 1587–1599.

(32) Penfound, T.; Foster, J. W. Biosynthesis and Recycling of NAD. In *Escherichia coli and Salmonella*; 1996.

(33) Tritz, G. J.; Chandler, J. L. R. Recognition of a Gene Involved in the Regulation of Nicotinamide Adenine Dinucleotide Biosynthesis. *Journal of Bacteriology* **1973**, *114*, 128–136.

(34) Penfound, T.; Foster, J. W. NAD-Dependent DNA-Binding Activity of the Bifunctional NadR Regulator of *Salmonella typhimurium*. *Journal of Bacteriology* **1999**, *181*, 648-655.

(35) Mortarino, M.; Negri, A.; Tedeschi, G.; Simonic, T.; Duga, S.; Gassen, H. G.; Ronchi, S. L-Aspartate oxidase from *Escherichia coli* I. Characterization of coenzyme binding and product inhibition. *European Journal of Biochemistry* **1996**, *239*, 418–426.

(36) Saxton, R. E.; Rocha, V.; Rosser, R. J.; Andreoli, A. J.; Shimoyama, M.; Kosaka, A.; Chandler, J. L.; Gholson, R. K. A comparative study of the regulation of nicotinamide-adenine dinucleotide biosynthesis. *Biochimica et biophysica acta* **1968**, *156*, 77–84.

(37) McLaren, J.; Ngo, D. T. C.; Oliveria, B. M. Pyridine Nucleotide Metabolism in *Escherichia coli* III. Biosynthesis from Alternative Precursors *in vivo*. *The Journal of biological chemistry* **1973**, *248*, 5144–5149.

(38) Gazzaniga, F.; Stebbins, R.; Chang, S. Z.; McPeek, M. A; Brenner, C. Microbial NAD metabolism: lessons from comparative genomics. *Microbiology and molecular biology reviews : MMBR* **2009**, *73*, 529–541.

(39) Gerdes, S. Y.; Scholle, M. D.; D'Souza, M.; Bernal, A.; Baev, M. V.; Farrell, M.; Kurnasov, O. V.; Daugherty, M. D.; Mseeh, F.; Polanuyer, B. M.; Campbell, J. W.; Anantha, S.; Shatalin, K. Y.; Chowdhury, S. A. K.; Fonstein, M. Y.; Osterman, A. L. From Genetic Footprinting to Antimicrobial Drug Targets : Examples in Cofactor Biosynthetic Pathways From Genetic Footprinting to Antimicrobial Drug Targets : Examples in Cofactor Biosynthetic Pathways. *Journal of bacteriology* **2002**, *184*, 4555–4572.

(40) Sassetti, C. M.; Boyd, D. H.; Rubin, E. J. Genes required for mycobacterial growth defined by high density mutagenesis. *Molecular microbiology* **2003**, *48*, 77–84.

(41) Schippers, J. H. M.; Nunes-Nesi, A.; Apetrei, R.; Hille, J.; Fernie, A. R.; Dijkwel, P. P. The *Arabidopsis onset of leaf death5* mutation of quinolinate synthase affects nicotinamide adenine dinucleotide biosynthesis and causes early ageing. *The Plant cell* **2008**, *20*, 2909–2925.

(42) Griffith, G. R.; Chandler, J. L.; Gholson, R. K. Studies on the *de novo* Biosynthesis of NAD in *Escherichia coli*. *European Journal of Biochemistry* **1975**, *245*, 239–245.

Chapter 2

Efforts to show a protein–protein interaction between NadA and NadB

2.1 Introduction

In the *de novo* biosynthesis of NAD in prokaryotes and most plants, a two-enzyme pathway forms quinolinic acid (QA), the first common intermediate in NAD biosynthesis in all organisms. The two enzymes were originally characterized in crude extract and the requirement for substrates and enzyme cofactors was ambiguous (*1*). Subsequent studies showed a requirement for L-aspartate and glycerol to produce QA in crude extract (*2*). While Gholson and coworkers observed the incorporation of ^{14}C into the QA carbon backbone when feeding *E. coli* with U-^{14}C-L-aspartate, feeding experiments with ^{14}C-labeled glycerol did not produce ^{14}C-labeled QA. This later study showed that the 3-carbon substrate for the reaction was either dihydroxyacetone phosphate (DHAP), now known as the true substrate of the enzyme, or 3-phosphoglyceraldehyde (G-3-P) (*3*).

Details of this *de novo* biosynthetic pathway of NAD were elucidated in the 1980's by Nasu and Gholson (*4*). The researchers observed the product of NadB reaction was identical to the product obtained from a D-aspartate oxidase catalyzed reaction. Either of these enzymes could support *in vitro* production of QA when mixed with crude extract containing NadA and DHAP. Further, oxaloacetate and an ammonium source could replace the NadB reaction *in vitro* to form QA in a reaction containing NadA and DHAP (*5*). These findings supported the product of the NadB reaction to be iminoaspartate (IA) and NadB is formally named L-aspartate oxidase. The oxidation of L-aspartate by NadB uses a non-covalently bound FAD molecule (*6*).

Reoxidation of the flavin cofactor can be performed by oxidization of molecular oxygen or under anaerobic conditions − fumarate. This yields hydrogen peroxide or succinate, respectively.

The first attempts to isolate NadA were carried out by refolding insoluble protein from inclusion bodies. This preparation yielded 12 mg/L culture of pure protein that catalyzed the formation of QA from the condensation reaction of IA and DHAP under aerobic conditions (*7*). Five years later, it was demonstrated that *E. coli* NadA contained a [4Fe-4S] that is required for catalysis (*8, 9*). This metal cofactor is oxygen-labile and the enzyme supported the complete cofactor and the fastest turnover under strict anaerobic conditions. Fortuitously while performing site-directed mutagenesis studies to investigate the cysteines that ligate the Fe/S cluster, it was discovered that two cysteines in *E. coli* NadA form a disulfide bond (*10, 11*). Though isolation and characterization of NadA has greatly improved, the mechanism by which NadA catalyzes QA formation is still unknown.

The NadB product, IA, was unable to be isolated and characterized from cells lacking the *nadA* gene (*ΔnadA*), and therefore it was postulated that the two enzymes function optimally when in a complex. Though no experimental evidence of a complex was noted, it was suggested this complex formed transiently, as active enzymes were isolated individually from a WT strain of *E. coli* (*12*). When cellular extracts of *ΔnadB* cells and *ΔnadA* cells were isolated independently and mixed, QA production was not observed. This observation suggested that a third gene product was involved in QA biosynthesis, or that knocking out one of the genes disrupted the function or activity of the protein encoded by the second gene (*13*). More recent evidence indicates that NadA and NadB are the only enzymes required for *de novo* synthesis of QA *(6)*. While the biosynthesis of NAD begins with NadB and NadA, there remains a lack of concrete data in support of a protein-protein interaction between the enzymes.

As the detailed *in vitro* characterization of *E. coli* NadB and *E. coli* NadA was carried out, no clear evidence of a complex between the two enzymes was found (*4*); however,

investigators were still probing this possible protein-protein interaction with new data that would arise. In a study of NadA and NadB from *B. subtilis*, NadA was separately bound to a His-tag and GST-affinity columns, which was mixed with crude lysate from cells over-expressing *B. subtillis* NadB was mixed with the resin. SDS-PAGE with analysis by silver staining showed that NadB eluted with the NadA eluate after extensive washing, indicating that some type of interaction (*14*). Work by Saunders indicates that *E. coli* NadB lacking any type of affinity tag does bind to affinity columns, including Ni-NTA (unpublished data). This observation suggests possibility that the purported interaction between *B. subtilis* NadA and NadB was via nonspecific binding of NadB to the columns. In the same study *of B. subtilis* enzymes, the researchers could not isolate the NadB-NadA complex by analytical molecular sieve chromatography where NadA and NadB were mixed in 1:1 or 2:1 ratio in the presence of excess dithionite and high salt (*14*). Furthermore, they showed that *B. subtilis* NadA kinetics did not change when IA was generated by *E. coli* NadB or *B. subtilis* NadB, indicating that NadA does not make physical contact with the NadB enzyme to acquire IA or *E. coli* NadB is capable of making the same contacts of *B. subtilis* NadB. Deviating from the previous data, when NadB binds IA and is mixed with NadA, the release of IA from the NadB is was observed to be facilitated by NadA, suggesting that the presence of NadA changes the affinity of NadB for IA (*14*). The mounting contradictory evidence of a protein-protein interaction only seemed to become more complicated with increasing knowledge of the individual enzymes.

The presence of disulfide bonds in NadAs from several species may provide insight into how the redox-sensitive enzymes interact to support NAD biosynthesis. In *E. coli* and *M. tuberculosis* NadAs, the presence of at least one disulfide bonds increases QA production *(8, 9)*. This redox trigger may be physiologically relevant, given that the disulfide-bond redox potential in *E. coli* NadA was determined to be – 264 mV (*11*) which is similar to that of the cytosol in *E. coli* (*15*). The oxidative potential of the cell may also be altered by NadB activity, since the

enzyme is one of the major producers of hydrogen peroxide in the cell (*16*). Additionally, growth conditions impact the levels of NAD related metabolites. Under aerobic growth, *E. coli* increases pools of NAD metabolites, which may be related to NadA's disulfide bond (*17*). Whether the oxygen-dependent nature of NadB is a regulatory mechanism for cellular NAD biosynthesis or solely QA production has yet to be determined.

This work attempts to demonstrate a protein-protein interaction between *E. coli* NadB and *E. coli* NadA by a number of biophysical and biochemical experiments. These studies focus on creating the NadB product complex, which consists of IA bound with the flavin cofactor in the reduced form, as this would be the state with which NadA is most likely to form a complex if the complex is transient. Setbacks, including the aerobic nature of most instrumentation and instability of the enzymes, prevented any definitive result supporting or disputing the suspected protein-protein interaction between NadB and NadA.

2.2 Materials and Methods

Materials. *Escherichia coli* genomic DNA (strain W3110), dihydroxyacetone phosphate (dilithium salt), and oxaloacetate was obtained from Sigma (St. Louis, MO). Coomassie blue dye-binding reagent for protein concentration determination and the bovine serum albumin (BSA) standard (2 mg mL^{-1}) and nitrobluetetrazolium chloride (NBT) were obtained from Pierce (Rockford, IL). Nickel nitrilotriacetic acid (Ni-NTA) resin was purchased from Qiagen (Valencia, CA). Sephadex G-25 resin and PD-10, NICK and NAP pre-poured gel filtration columns were purchased from GE Biosciences (Piscataway, NJ). 2,3-Pyridinedicarboxylic acid (QA standard) was obtained from Aldrich (St. Louis, MO). AP-Goat Anti-Rabbit IgG (H & L) was obtained from Invitrogen (Grand Island, NY). 5-bromo-4-chloro-3'-indolylphosphate (BCIP) was purchased from VWR International (West Chester, PA). All other buffers and chemicals were of the highest grade available.

General Procedures. High performance liquid chromatography (HPLC) was conducted on a Beckman System Gold unit (Fullerton, CA), which was fitted with a 128 diode array detector and operated with the System Gold *Nouveau* software package. UV-visible spectra were obtained on a Cary 50 spectrometer (Varian; Walnut Creek, CA) using the associated WinUV software package. Iron and sulfide analysis was performed as previously described (*18–20*). Sonic disruption of *E. coli* cells was carried out with a 550 sonic dismembrator from Fisher Scientific (Pittsburgh, PA) in combination with a horn containing a ½ in. tip. The horn was threaded through a port in an anaerobic chamber to allow the process to be conducted under anoxic conditions. Procedures conducted under anaerobic conditions were carried out in an anaerobic chamber from Coy Laboratory Products, Inc. (Grass Lake, MI) under an atmosphere of N_2 and H_2 (95% / 5%), with an O_2 concentration maintained below 1 ppm by the use of palladium catalysis.

Enzymes were prepared in the same manner as previously described (*21*). WT and E288Q EcNadA were over-expressed from *E. coli* BL21(DE3), purified anaerobically via immobilized metal affinity chromatography (IMAC), and reconstituted as previously described (*21*, *22*).

Steady State Assays with EcNadA$_{ox}$ with OAA and NH$_4$Cl in the presence of NadB. WT EcNadA RCN was exchanged into gel filtration buffer lacking DTT (50 mM HEPES pH 7.5, 0.1 M KCl, 20 % glycerol) using a NICK gel filtration column. Protein determination was carried out by Bradford and NadA (5 µM) was incubated in a reaction containing 200 mM HEPES, pH 7.5 with 200 µM Trx_{ox} at 37 °C for 20 min anaerobically. After the incubation period, 0.1 M KCl, 0.1 M NH_4Cl, 1 mM DHAP, 0.3 mM Trp (IS), 25 µM FAD and various concentrations of NadB were added. The reaction mixture was incubated for 3 min at 37 °C before the addition of 10 mM OAA. Every minute, 200 µL of reaction mixture was quenched into 40 µL of 2 M trichloroacetic acid (TCA). The resulting sample was centrifuged for 30 min at 14,000 × *g* and the supernatant was analyzed by HPLC as previously described to quantify QA (*21*).

Aerobic assays were performed in the same manner after the enzyme was buffer exchanged by gel filteration anaerobically. The enzyme solution was removed from the glove box and allowed to equilibrate at room temperature for 20 min. The reaction was initiated with 5 mM OAA and 200 µL of the reaction mixture was quenched into 40 µL 2 M TCA every 2 min.

Monitoring $FADH_2$ oxidation by Stopped-Flow Spectroscopy. Anaerobic single mix stopped-flow spectroscopy was carried out as described previously (*23*). In a buffered solution of 50 mM HEPES, pH 7.5, 100 µM NadB was reduced instantaneously with 1 equivalent of dithionite (100 µM) and loaded into syringe. In another syringe 30 mM fumarate, pH 8.0 was loaded. A control mixing experiment was performed with anaerobic 50 mM HEPES, pH 7.5, in place of fumarate.

Monitoring heat of mixing of NadB and NadA by isothermal calorimetry (ITC). WT EcNadA and EcNadB were buffer-exchanged into 50 mM HEPES, pH 7.5, 0.15 M KCl, 10% glycerol using pre-poured NAP columns. The resulting protein was concentrated using Amicon YM-10 membrane. ITC experiments were performed on a VP-ITC (MicroCal, Inc., Northampton, MA) as previous described (*24*). Samples were degassed at 35 °C for 10 min prior to being loaded into the instrument. Titration data were integrated and analyzed using Origin (OriginLabCorp., Northampton MA).

Apo-NadA overexpression and purification. Apo-NadA was prepared by over-expression of EcNadA from a pET28a-derived plasmid in BL21(DE3), lacking the pDB1282 plasmid from *Azotobacter vindelandii* which promotes Fe/S cluster formation. The cells were incubated in 16 L of M9 minimal media until an OD_{600}= 0.6 at which point IPTG was added to a final concentration of 200 µM, and the cells were incubated for an additional four hours. The cells were harvested by centrifugation and stored in liquid N_2. Purification was carried out as described previously (*21*). Apo-[U-^{15}N]-labeledNadA was over-expressed as described above, except the M9 minimal media contained $^{15}NH_4Cl$.

^{15}N-labeled NadA overexpression and purification. pET28a-EcNadA containing the pDB1282 plasmid from *A. vindelandii* was over-expressed in M9 minimal media containing $^{15}NH_4Cl$ in 8 L. At an OD_{600}= 0.3, arabinose was added to a final concentration 0.2 %. At OD_{600}= 0.6, the flasks were placed in an ice/water bath and chilled for 20 min. IPTG (200 µM) and $FeCl_3$ (50 µM) were added, and the cultures were incubated overnight at 18 °C. The cells were harvested by centrifugation and stored in liquid N_2. Purification was carried out as described previously (*21*).

Samples for NMR were prepared by buffer exchanging the protein into 50 mM HEPES, pH 7.5, 0.1 M KCl, 10 mM DTT using a pre-poured NAP column and concentrating the protein using a Microcon Centrifugal Filter Device (Millipore Ultracel YM-10 membrane) anaerobically to a final concentration of 1 mM in a volume of approximately 500 µL. To the sample, 50 µL D_2O was added and the tube was sealed with parafilm in the anaerobic chamber. To the ^{15}N-labeled NadA samples, a 1.2 molar equivalent of NadB, in the analogous buffer, was added to the tube after the individual NadA spectra were recorded. Data (^{1}H-^{15}N HSQC) was collected on an 850 MHz (20.0T) US2 Avance III Spectrometer equipped with a TCI-Cryoprobe.

Western Blots. Rabbit antibodies were produced by GenScript (Piscataway, NJ) using an antigenic peptide sequence unique to each enzyme: NH_2-CPPWDESRVENPDER-COOH for NadB and CDKHLGRYVQKQTGG for NadA. Western blots were visualized using AP-Goat Anti-Rabbit IgG (H & L) secondary antibodies with alkaline phosphatase reagents: nitrobluetetrazolium chloride (NBT) and 5-bromo-4-chloro-3'-indolyphosphate (BCIP).

Briefly, unboiled samples were separated on 12% SDS-PAGE and blotted onto a PVDF membrane. All membrane washing steps took place at 4 °C on a rocker platform. The membrane was incubated in 1:1000 1° antibody (Rabbit Anti-NadA or Anti-NadB) solution in a 5% BSA, TBS blocking solution for one hour. After TBSTT and TBS washes, the membrane was incubated in 1:5000 2° antibody (Goat Anti-Rabbit IgG) solution for one hour. Developing

solutions of NBT and BCIP were made fresh in 1 × AP buffer, and the membrane was incubated in this solution for under five min to visualize bands.

2.3 Results

$NadA_{ox}$ Activity. To observe substrate channeling between NadB and NadA, two sets of assays were performed in which NadA was oxidized by two different oxidants: oxidized Trx or molecular oxygen (O_2). When $NadA_{ox}$ was given excess IA − by the Schiff's base reaction with OAA and NH_4Cl − in the presence of various concentrations of NadB, the activity of NadA was inhibited by the presence of NadB. The NadB concentrations were near-stoichiometric to NadA concentrations so that a 1:1 complex could be generated if NadB channeled IA directly to NadA. NadA can obtain IA from solution *(4)*; however, it was hypothesized that NadA prefers to obtain IA from NadB via some type of protein-protein interaction especially at low IA concentrations. The decreasing QA production with increasing concentrations of NadB supports that NadB blocks NadA from binding IA from solution (Figure 2-1). This result is consistent under aerobic and anaerobic conditions, suggesting the enzyme association is independent of oxygen.

While the activity of *E. coli* NadA in the presence of oxidants has previously been determined *(9)*, the presence of the disulfide bond on NadA may elicit binding to NadB or affect its binding of IA. Though oxidized thioredoxin provides a more gentle method for generation of the disulfide bond on NadA, given that it does not damage the Fe/S cluster, oxygen supports faster turnover of NadB than fumarate which it uses to reoxidize its reduced flavin cofactor under anaerobic conditions. This behavior arises because fumarate binds at the same site as does Asp or IA, causing it to impact the activity of the protein in a competitive fashion. The higher turnover of NadB in the presence of oxygen may conceivably impact the ability of NadA to obtain IA, given that it should be produced at higher concentrations. The aerobic assays support the same conclusion from the anaerobic assays, in that NadB suppresses NadA activity.

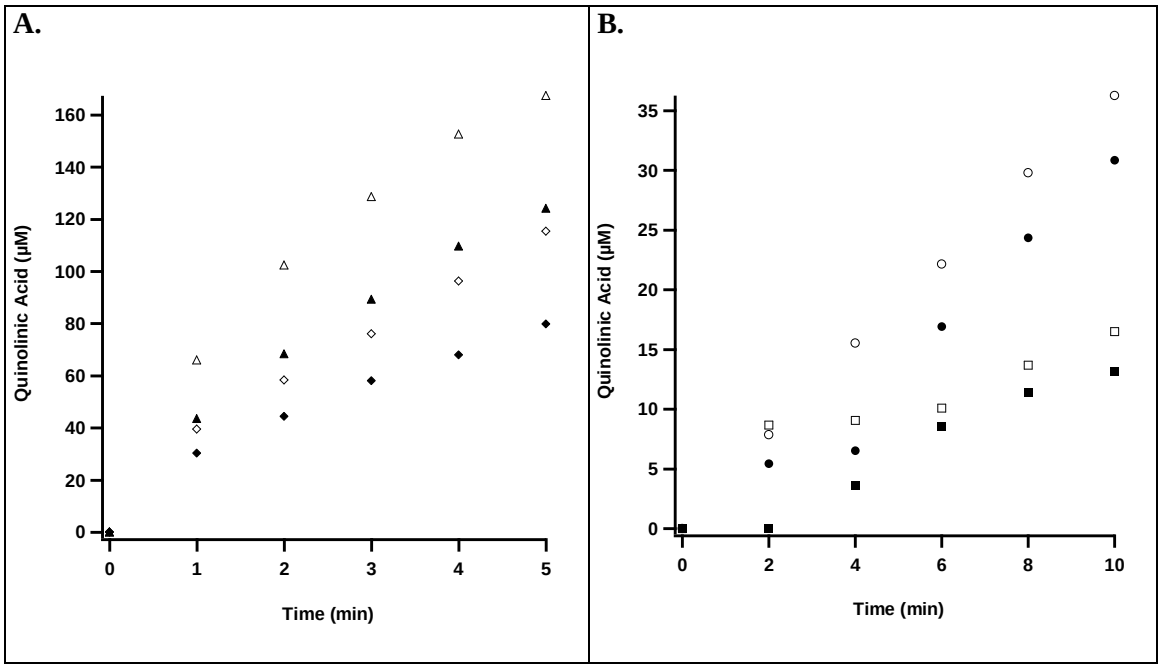

Figure **2-1**: Oxidized NadA activity with OAA/NH_4Cl in the presence of NadB.

NadA treated with Trx_{ox} anaerobically. Control/0 µM NadB (open triangles), 10 µM NadB (closed triangles), 20 µM NadB (open diamonds), 30 µM NadB (closed diamonds) (Panel A).

NadA assayed aerobically. Control/0 µM NadB (open circles), 1 µM NadB (closed circles), 5 µM NadB (open squares), 10 µM NadB (closed squares) (Panel B).

Stopped-flow rapid mixing and UV/Vis-spectroscopy of NadB product complex. In single mixing stopped-flow experiments, NadB bound with IA and $FADH_2$ was mixed against fumarate to determine the rate of oxidation of the flavin cofactor. NadB was reduced by adding small aliquots of dithionite and observing the flavin absorbance decrease (at 452 nm), until the flavin spectrum was at a minimum and excess NH_4Cl and OAA were added to produce the NadB/IA product complex. NadB was oxidized at a rate of 0.07 s^{-1} when mixed against fumarate (Figure 2-2). In a control mixing experiment, NadB oxidation was observed when mixed against anaerobic buffer at a rate of 0.035 s^{-1}. Since NadB was oxidized by buffer, it was thought that the light source caused photooxidation. Additionally, the absorbance of the oxidized flavin did not

return to its starting value when the protein was mixed with excess fumarate, suggesting that a portion of the enzyme was compromised by reduction with dithionite.

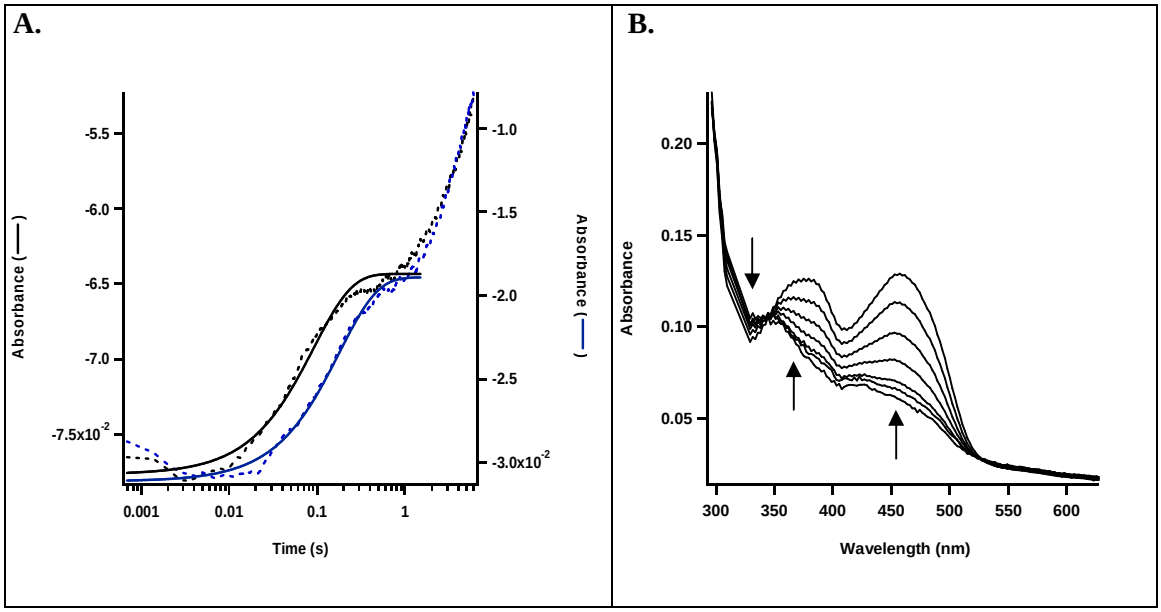

Figure **2-2**: Stopped-Flow Spectra of EcNadA. Oxidation of NadB upon mixing with fumarate (black) or buffer (blue) (Panel A). Photodiode array data of the flavin spectrum growing in upon oxidation with fumarate (Panel B).

Evidence of a NadB-NadA complex by ITC. To observe a protein-protein interaction in solution, a series of titrations were performed to measure the heat of binding of the two enzymes. In a titration where NadA, acting as the ligand, was titrated into NadB, a heat release was seen approaching a 1:1 ratio of NadB to NadA (Figure 2-3). Upon completion of the titration, it was seen that most of the protein had precipitated in the cell; however, it was unclear if the precipitation occurred during or after the titration. In attempt to isolate the source of the precipitation, control titrations were performed where NadA and NadB were individually titrated into buffer (Figure 2-3). While the heat release for each of the controls was less than the heat release observed when one enzyme was titrated against other, significant precipitation was still

observed. It was thought that NadA, oxidized by atmospheric oxygen, would be able to withstand the oxic environment; however, the highly concentrated solution of protein needed in the experiment may have contributed to the instability of the enzymes.

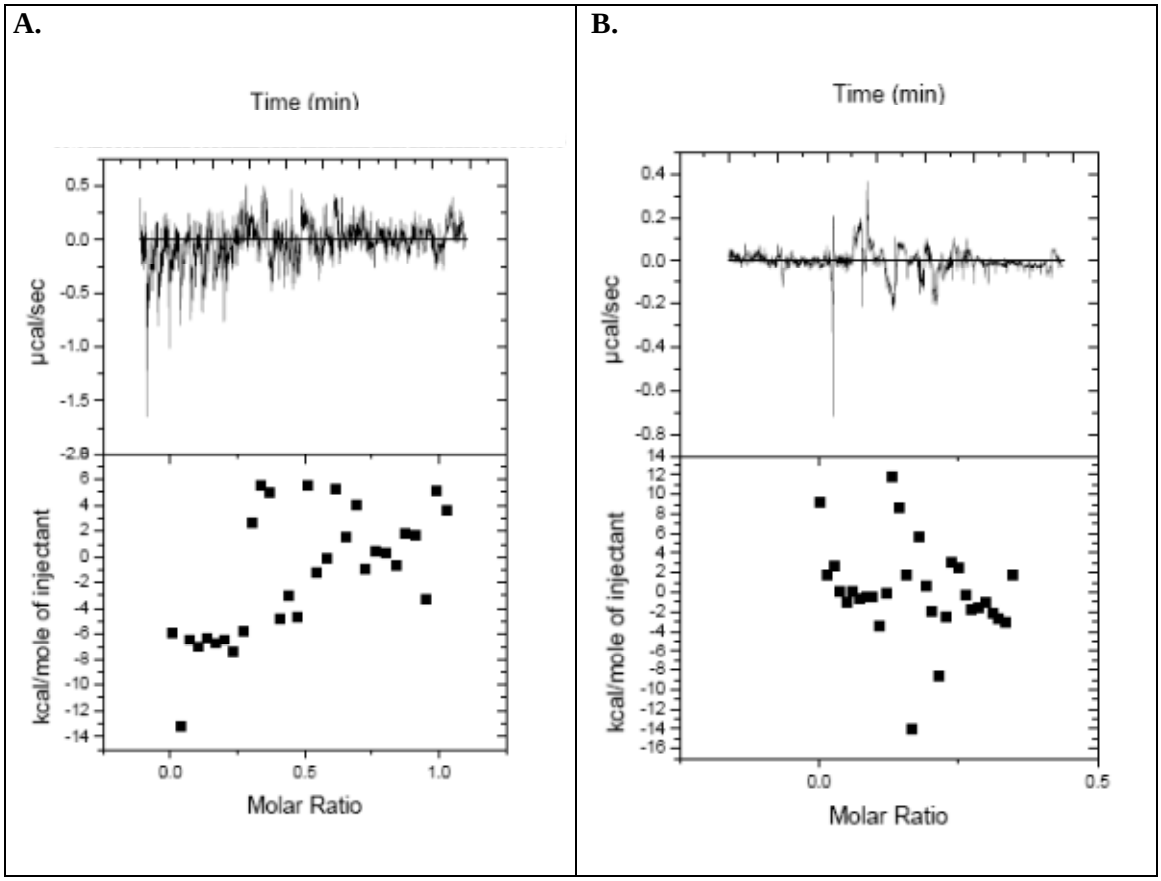

Figure **2-3**: ITC data. WT EcNadA titrated into WT EcNadB (Panel A). WT EcNadA titrated into buffer (Panel B).

Evidence of a NadB-NadA complex by high-field NMR. Expression of *nadA*, with co-expression of the *isc* operon encoded on the pDB1282 plasmid, in ^{15}N-enriched M9 minimal media produced cell yields similar to that to Saunders *et al.*, and the ^{15}N-labeled proteinwas purified via affinity chromatography (Ni-NTA) (*8*). The ^{15}N-labeled holo-enzyme was

reconstituted as described previously (*16*) and yielded 10.84 mg of holo-enzyme (3.2 ± 0.6 Fe/polypeptide) per 1 g cell paste. NadA lacking the Fe/S cluster (apo-NadA) was produced by expression in minimal media in the absence of the pDB1282 plasmid and without $FeCl_3$ supplementation to the media during the bacterial growth. The yield of ^{15}N-labeled apo-NadA was 1.4 mg per 1 g cell paste with 0.26 ± 0.08 Fe/polypeptide, while the yield of unlabeled apo-NadA was produced 0.34 mg protein per 1 g cell paste with 0.6 ± 0.3 Fe/polypeptide. The ^{15}N-HSQC NMR spectrum from the apo-enzyme showed an abundance of signals near 8.3 ppm indicating a disordered protein, while the ^{15}N-labeled holo-NadA showed a more dispersed signal typical of an ordered or properly folded protein. The spectrum containing holo-enzyme had some signals that were bleached, because of thermally populated paramagnetic states of the $[4Fe\text{-}4S]^{2+}$ cluster. The ^{15}N-labeled holo NadA in the presence of NadB showed little signal. The NadB-NadA protein complex would have created a macromolecule of nearly 100 kDa, which approaches the limit of what can be observed with present technology due to slow tumbling of the complex.

Preliminary Background for the Investigation of a NadB-NadA complex by Western Blot/Pull Down. To test the specificity of the enzyme-specific antibodies, western blot controls were performed with purified enzymes. Individually, NadA and NadB were separated by 12% SDS-PAGE and then transferred to a membrane before analyzing with anti-NadA and anti-NadB antibodies. No cross reactivity, of the anti-NadA antibody bound to NadB or vice versa was observed (Figure 2-3, Panel B, C). Incubation of BL21 cells without IPTG induction of EcNadA from the pET28a plasmid resulted in low level of expression of enzyme that produced a clear band when blotted against anti-NadA (Figure 2-3, Panel A). Pull-down experiments where NadA can be isolated at a basal level of expression and blotted to examine whether NadB is isolated with NadA need to be performed to confirm a NadB-NadA complex *in vivo*.

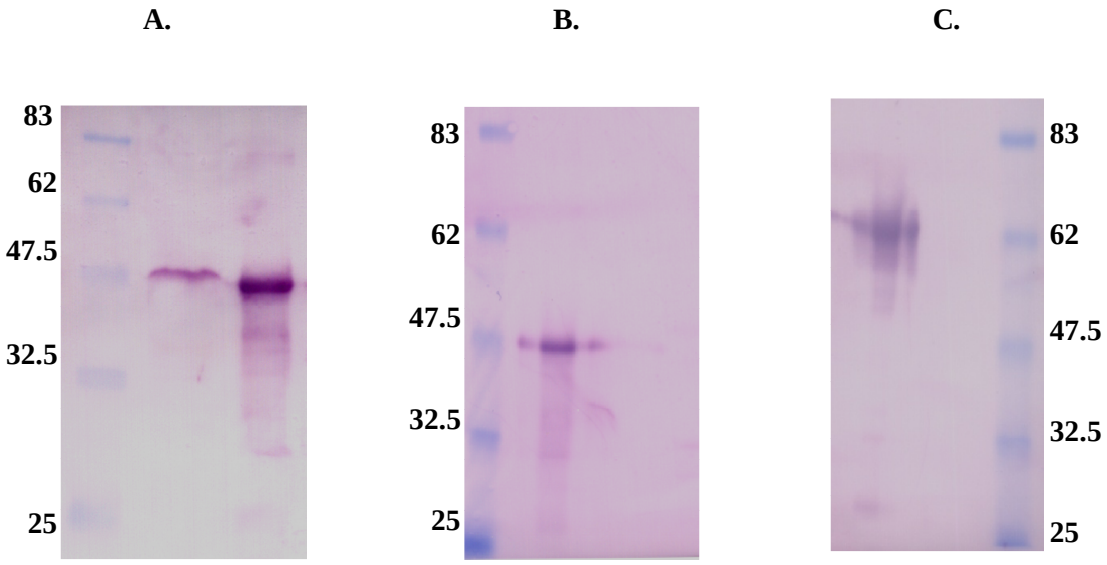

Figure **2-3:** Western Blots (Panel A) Anti-NadA WB. Lanes: **1**, molecular weight markers; **2**, BL21 pET28a EcNadA; **3**, pure EcNadA (MW = 45kDa). (Panel B) Anti-NadA WB. Lanes: **1**, molecular weight markers; **2**, pure EcNadA; **3**, pure NadB (MW = 66 kDa). (Panel C) Anti-NadB WB. Lanes: **1**, pure NadB; **2**, pure NadA; **3**, molecular weight markers.

2.4 Discussion

While some studies suggest that NadA and NadB interact to facilitate QA production, none are supported concrete unambiguous data. Herein, many experiments have shown the difficulty of working with two enzymes with redox sensitive cofactors. Attempts to observe the protein-protein interaction of NadB and NadA were unsuccessful due to a number of experimental conditions. The relatively high protein concentrations required for some of the methods caused the enzymes to precipitate. The inability to perform many of the experiments in an anaerobic environment also hindered the outcome of several experiments. While NadA was kept anaerobic for as long as possible to maintain the integrity of the Fe/S cluster, under certain conditions aerobiosis caused precipitation.

It also remains unclear if *E. coli* NadA can signal release of IA from NadB. With the presence of the disulfide bond in *E. coli* NadA, QA production increases thus possibly signaling NadB to release, or increase turnover of IA. The NadB kinetics demonstrate that the rate limiting step in the reaction may be the release of IA and reoxidation of NadB. Oxygen, as the oxidizing agent, can increase NadB turnover since it does not compete with the IA active site unlike fumarate. Monitoring IA release by NadB will not show if substrate channeling is occurring as the rate of release is not the rate limiting step in the reaction.

Other techniques to monitor this protein-protein interaction could be more successful with instrumentation that maintains an anaerobic environment. Additionally, a highly sensitive liquid chromatography-mass spectrometry (LC-MS) assay was developed after the completion of these studies, which would allow for isotopic labeling experiments to be carried out. These experiments would show if IA is released from NadB, so that it competes with isotopically labeled NH_4Cl or OAA in solution. The resulting QA which would either contain labeled moieties from the IA from solution or unlabeled from the L-aspartate transformation from NadB could be analyzed by LC-MS. Additionally, *in vivo* complementation experiments have been ongoing, yet have not provided a resolve in the controversy of the NadB-NadA protein-protein interaction *(7, 9, 22)*.

2.5 References

(1) Ortega, M. V.; Brown, G. M. Precursors of nicotinic acid in *Escherichia coli*. *The Journal of biological chemistry* **1960**, *235*, 2939–2945.

(2) Saxton, R. E.; Rocha, V.; Rosser, R. J.; Andreoli, A. J.; Shimoyama, M.; Kosaka, A.; Chandler, J. L.; Gholson, R. K. A comparative study of the regulation of nicotinamide-adenine dinucleotide biosynthesis. *Biochimica et biophysica acta* **1968**, *156*, 77–84.

(3) Chandler, J. L., Gholson, R. K. Studies on the Biosynthesis of NAD in *Escherichia coli* iii. Precursors of Quinolinic Acid *in vitro*. *Biochemica and Biophysica Acta* **1971**, *264*, 311–318.

(4) Nasu, S.; Wicks, D.; Gholson, R. K. L-Aspartate Oxidase, a Newly Discovered Enzyme of *Escherichia coli*, Is the B protein of Quinolinate Synthetase. *J. Biol. Chem.* **1982**, *257*, 626–632.

(5) Nasu, S., Gholson, R. K. Replacement of the B protein Requirement of the *E. coli* Quinolinate Synthetase System by Chemically-Generated Iminoaspartate. *Biochemical and Biophysical Research Communications* **1981**, *101*, 533–539.

(6) Mortarino, M.; Negri, A.; Tedeschi, G.; Simonic, T.; Duga, S.; Gassen, H. G.; Ronchi, S. L-Aspartate oxidase from *Escherichia coli* I. Characterization of coenzyme binding and product inhibition. *European Journal of Biochemistry* **1996**, *239*, 418–426.

(7) Ceciliani, F.; Caramori, T.; Ronchi, S.; Tedeschi, G.; Mortarino, M.; Galizzi, a Cloning, overexpression, and purification of *Escherichia coli* quinolinate synthetase. *Protein expression and purification* **2000**, *18*, 64–70.

(8) Cicchillo, R. M.; Tu, L.; Stromberg, J. A.; Hoffart, L. M.; Krebs, C.; Booker, S. J. *Escherichia coli* quinolinate synthetase does indeed harbor a [4Fe-4S] cluster. *Journal of the American Chemical Society* **2005**, *127*, 7310–7311.

(9) Ollagnier-de Choudens, S.; Loiseau, L.; Sanakis, Y.; Barras, F.; Fontecave, M. Quinolinate synthetase, an iron-sulfur enzyme in NAD biosynthesis. *FEBS letters* **2005**, *579*, 3737–3743.

(10) Rousset, C.; Fontecave, M.; Ollagnier de Choudens, S. The [4Fe-4S] cluster of quinolinate synthase from *Escherichia coli*: investigation of cluster ligands. *FEBS letters* **2008**, *582*, 2937–2944.

(11) Saunders, A. H.; Booker, S. J. Regulation of the Activity of *Escherichia coli* Quinolinate Synthase by Reversible Disulfide-Bond Formation. *Biochemistry* **2008**, *47*, 8467–8469.

(12) Griffith, G. R.; Chandler, J. L.; Gholson, R. K. Studies on the *de novo* Biosynthesis of NAD in *Escherichia coli*. *European Journal of Biochemistry* **1975**, *245*, 239–245.

(13) Tritz, G. J.; Chandler, J. L. R. Recognition of a Gene Involved in the Regulation of Nicotinamide Adenine Dinucleotide Biosynthesis. *Journal of Bacteriology* **1973**, *114*, 128–136.

(14) Marinoni, I.; Nonnis, S.; Monteferrante, C.; Heathcote, P.; Härtig, E.; Böttger, L. H.; Trautwein, A. X.; Negri, A.; Albertini, A. M.; Tedeschi, G. Characterization of L-aspartate oxidase and quinolinate synthase from *Bacillus subtilis*. *The FEBS journal* **2008**, *275*, 5090–5107.

(15) Gilbert, H. F. Molecular and cellular aspects of thoil-disulfide exchange. *Adv. Enzymol. Relat. Areas Mol. Biol.* **1990**, *63*, 69–72.

(16) Korshunov, S.; Imlay, J. A. Two sources of endogenous hydrogen peroxide in *Escherichia coli*. *Molecular microbiology* **2010**, *75*, 1389–1401.

(17) Wimpenny, J. W.; Firth, A. Levels of nicotinamide adenine dinucleotide and reduced nicotinamide adenine dinucleotide in facultative bacteria and the effect of oxygen. *Journal of bacteriology* **1972**, *111*, 24–32.

(18) Beinert, H. Micro Methods for the Quantitative Determination of Iron and Copper in Biological Material. *Methods Enzymol* **1978**, *54*, 435–445.

(19) Beinert, H. Semi-micro methods for analysis of labile sulfide and of labile sulfide plus sulfane sulfur in unusually stable iron-sulfur proteins. *Analytical biochemistry* **1983**, *131*, 373–378.

(20) Kennedy, M. C.; Kent, T. A.; Emptage, M.; Merkle, H.; Beinert, H.; Münck, E. Evidence for the formation of a linear [3Fe-4S] cluster in partially unfolded aconitase. *The Journal of biological chemistry* **1984**, *259*, 14463–71.

(21) Saunders, A. H.; Griffiths, A. E.; Lee, K.-H.; Cicchillo, R. M.; Tu, L.; Stromberg, J. A.; Krebs, C.; Booker, S. J. Characterization of quinolinate synthases from *Escherichia coli*, *Mycobacterium tuberculosis*, and *Pyrococcus horikoshi*i indicates that [4Fe-4S] clusters are common cofactors throughout this class of enzymes. *Biochemistry* **2008**, *47*, 10999–11012.

(22) Saunders, A. H. Investigation of the Structure, Function, and Regulation of Quinolinate Synthase: The Iron-Sulfur Cluster Enzyme Involved in Prokaryotic NAD Biosynthesis, The Pennsylvania State University, 2011.

(23) Price, J. C.; Barr, E. W.; Tirupati, B.; Bollinger, J. M.; Krebs, C. The first direct characterization of a high-valent iron intermediate in the reaction of an alpha-ketoglutarate-dependent dioxygenase: a high-spin Fe^{IV} complex in taurine/alpha-ketoglutarate dioxygenase (TauD) from *Escherichia coli*. *Biochemistry* **2003**, *42*, 7497–7508.

(24) Sokoloski, J. E.; Bevilacqua, P. C. Analysis of RNA Folding and Ligand Binding by Conventional and High-Throughput Calorimetry. In *Bacterial Regulatory RNA: Methods and Protocols*; Keiler, K. C., Ed.; Humana Press: Totowa, NJ, 2012; Vol. 905, pp. 145–174.

Chapter 3

Efforts to show coordination of DHAP and Iminoaspartate to the Fe/S cluster of NadA

3.1 Introduction

NAD biosynthesis in most prokaryotes and some plants involves a two-enzyme pathway to form quinolinic acid (QA), the pyridine ring precursor of NAD. This pathway begins with the two-electron oxidation of L-aspartate by the enzyme L-aspartate oxidase (NadB) using non-covalently bound flavin adenine dinucleotide (FAD) as the electron acceptor. FAD is reformed upon transfer of reducing equivalents from $FADH_2$ to oxygen or fumarate which yields hydrogen peroxide or succinate. The product of the NadB reaction, iminoaspartate (IA), is then condensed with dihydroxyacetone phosphate (DHAP) by the action of quinolinate synthase (NadA). Though these two enzymes have been known for 20 years, the mechanism of NadA has not been resolved.

Once the substrate requirements of NadA were discovered, the first mechanism was proposed by Gholson and coworkers (Figure 3-1, Panel A) (*1*). This mechanism involves attacks of C3 of the enamine form of IA onto C1 of DHAP with concomitant release of inorganic phosphate. This species undergoes multiple keto/enol and imine/enamine tautomerizations to arrive at a species that gives rise to ring closure via Schiff's base formation. The last step of the mechanism is a dehydration to afford QA. Though not originally proposed by Gholson and coworkers, it has been postulated that this dehydration step involves Lewis acid catalysis via the action of a [4Fe–4S] cluster prosthetic group.

Begley and coworkers proposed another mechanism in which DHAP is initially converted to G-3-P (Figure 3-1, Panel B) (*2*). In this mechanism, the enamine form of IA

undergoes Schiff's base formation with the aldehyde of G-3-P. Removal of a proton from C2 of the G-3-P moiety of the resulting molecule — facilitated via resonance of the resulting carbanion into the iminium ion species — facilitates elimination of phosphate to set up an electrocyclic ring closure. Similiarly to the mechanism described previously, the last step is a dehydration reaction that is believed to be facilitated by a [4Fe-4S] cluster. One of the most notable differences in this mechanism is the release of the phosphate group later in the reaction mechanism. Attempts to determine whether phosphate release could be uncoupled from QA production to corroborate one of the mechanisms were not successful (*3*).

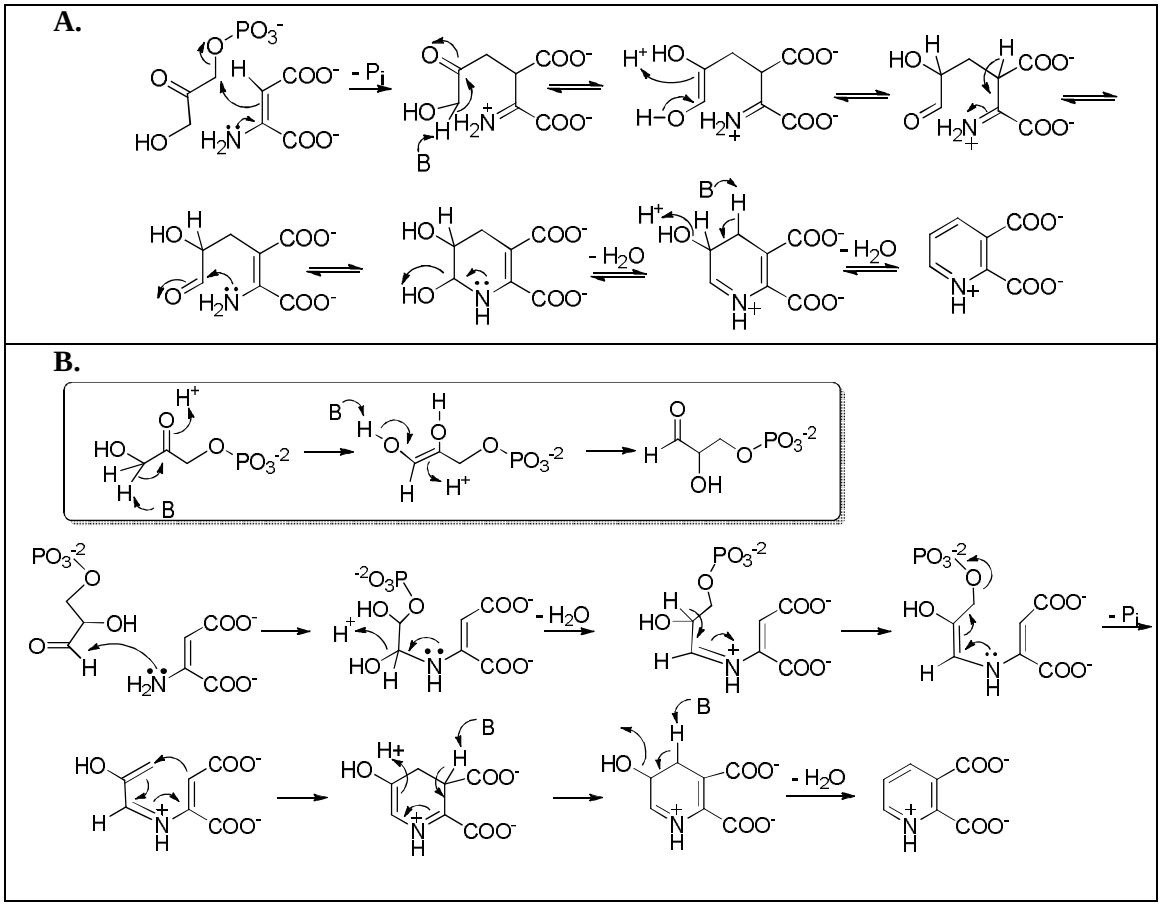

Figure **3-1**: Mechanisms proposed by Gholson (Panel A) (*1*) and Begley (Panel B) (*2*).

Though the two mechanisms differ in the steps to form the pyridine ring, they both include the final elimination of a water molecule to form QA. The discovery that NadA contains a metal cofactor was confirmed by two laboratories in 2005, and was thought to assist in this final dehydration (*4*, *5*). The characterization of a [4Fe-4S] cluster was carried out with spectroscopy, quantitative iron and sulfide analyses, and enzymatic activity determination. The three cysteines that ligate the cluster were determined by site-directed mutagenesis, in combination with activity and iron and sulfide assays (*6*, *7*). The unligated Fe, known as the unique iron site, likely assists in the final dehydration at C5 of the pyridine ring (Figure 3-2, Panel A). A recent study used an active site inhibitor that coordinates to the unique iron site as shown by Mössbauer spectroscopy and DFT calculations to provide evidence for the role of the [4Fe-4S] cluster in catalysis (*8*). The inhibitor, dithiolhydroxyphthalic acid (DTHPA), contains two thiol groups at C5 and C6 of the pyridine ring that binds bidentate to the unique iron site (Figure 3-2, Panel B). Because the location of one of the thiol moieties is identical to the location of the hydroxyl group that is eliminated as water in the last step of the NadA mechanism, it can be infered that the Fe/S cluster functions as a Lewis acid (*8*).

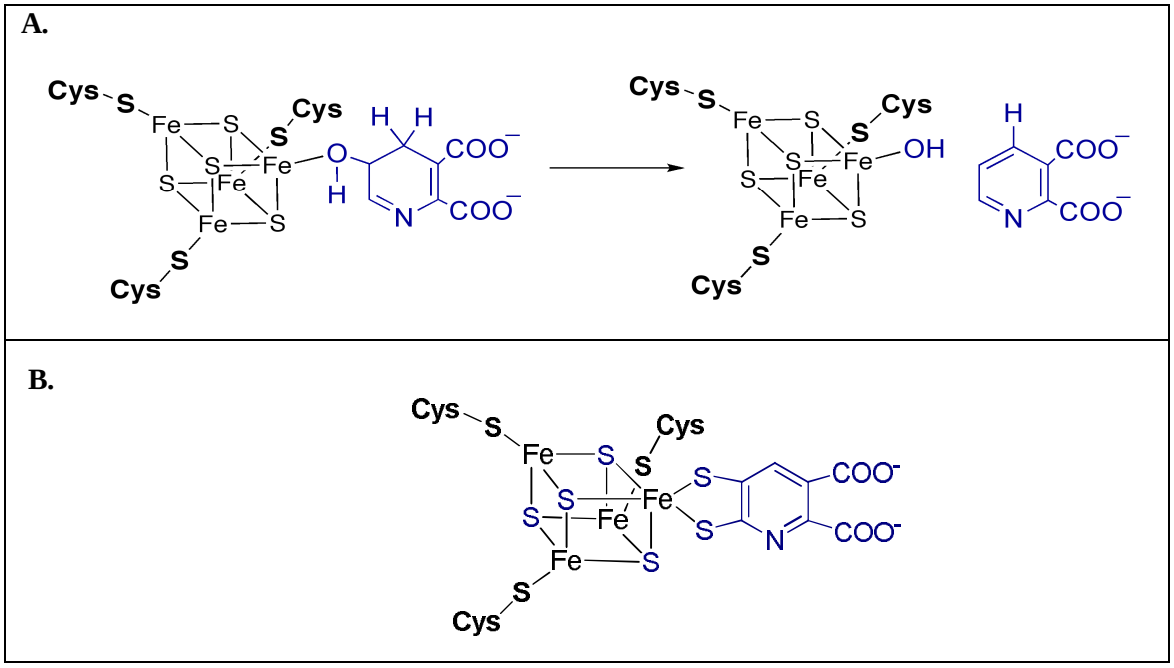

Figure **3-2**: Ligands of the unique iron site in the Fe/S cluster of NadA. Proposed role of the Fe/S cluster in NadA acting as a Lewis acid (Panel A) (*4*, *5*). Binding of dithiol inhibitor of NadA (Panel B) (*8*).

The prototypical member of the class of enzymes that function employ an Fe/S cluster as a Lewis acid is aconitase. As a well established member of the Fe-dependent hydrolyase class of enzymes, aconitase has been studied with various spectroscopic techniques in conjunction with appropriately labeled substrates and substrate analogs (*9*). This enzyme performs an isomerization of citrate to isocitrate via the intermediate cis-aconitate. The unique iron site of the [4Fe-4S] cluster binds the hydroxyl group to be eliminated and a carbonyl of the carboxylate group along with a molecule of water. The dehydrated intermediate intermediate, cis-aconitate, rebinds in the active site flipped 180° and the hydroxyl group adds to C2 to form isocitrate.

While it is presumed that the Fe/S cluster of NadA functions as a Lewis acid to aid in the final dehydration to form QA, no spectroscopic evidence has been reported of substrates or reaction intermediates binding the unique iron site. Perturbations in the EPR spectrum of NadA

when it is incubated with a number of substrates suggest that substrate/intermediate binding can be monitored through spectroscopic techniques (Figure 3-3). Specifically, the binding of IA to an *E. coli* NadA variant, E228Q, produces significant changes in the EPR signal of the reduced enzyme, with a tightening of the spectrum from rhombic to more axial. These differences are thought to arise from conformational changes in the protein upon binding of the substrate (*3*). Since IA produces spectral changes in the EPR spectrum, it is conceivable that IA binds to the iron site in a bidentate fashion via its two carboxylate groups.

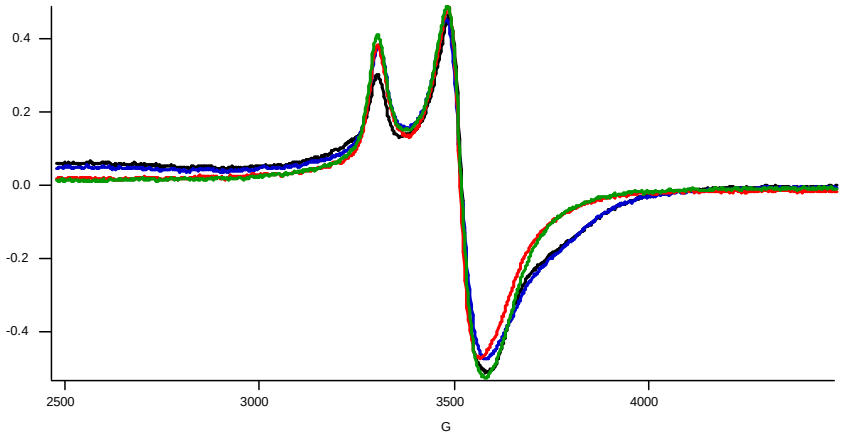

Figure **3-3**: EPR of *E. coli* NadA E228Q (black) in the presence of DHAP (blue), in the presence of IA (red), in the presence of both DHAP and IA (green) from Saunders (*3*).

3.2 Materials and Methods

Materials. Coomassie blue dye-binding reagent for protein concentration determination and the bovine serum albumin (BSA) standard (2 mg mL^{-1}) were obtained from Pierce (Rockford, IL). Nickel nitrilotriacetic acid (Ni-NTA) resin was purchased from Qiagen (Valencia, CA). Sephadex G-25 resin and PD-10, NAP, NICK pre-poured gel filtration columns were purchased from GE Biosciences (Piscataway, NJ). Anion exchange resin (AG 1X-2) was purchased from

Bio-Rad (Hercules, CA). Dihydroxyacetone phosphate (dilithium salt), oxaloacetate, α-glycerophosphate dehydrogenase (from rabbit muscle), pyruvate kinase (from rabbit muscle), malate dehydrogenase, lactate dehydrogenase (from bovine heart), catalase (from bovine liver), glycerol kinase (from *E. coli*), and L-glyercol-3-phosphate oxidase (from *Aerococcus viridians*) were obtained from Sigma Aldrich (St. Louis, MO). 2-^{13}C glycerol (99%) was purchased from Cambridge Isotope Laboratories (Andover, MA). All other buffers and chemicals were of the highest grade available.

General Procedures. HPLC with detection by mass spectrometry (LC-MS) was conducted on an Agilent Technologies (Santa Clara, CA) 1200 system, which was fitted with an autosampler for sample injection and coupled to an Agilent Technologies 6410 QQQ mass spectrometer. The system was operated with the associated MassHunter software package, which was also used for data collection and analysis. Samples (2 µL injections) were separated on an Agilent Technologies Zorbax SB-C18 column (2.4 mm × 35 mm, 3.5 µm particle size), which was equilibrated in 100% Solvent A (0.1% formic acid in water, pH 2.6) at a flow rate of 0.4 mL min^{-1}. A gradient of 0–20% acetonitrile was applied from 0.4 to 2 min, and then returned to 0% acetonitrile from 2 to 2.5 min. The column was allowed to re-equilibrate for 1.5 min under initial conditions before subsequent sample injections. Detection of DHAP (*m/z* = 171) was performed using electrospray ionization in positive mode (ESI$^+$) with multiple reaction monitoring (MRM). DHAP fragmentation was monitored at *m/z* = 99 at 0.5 min with a fragmentor energy of 40 V and collision energy of 10 V. Iron and sulfide analysis was performed as previously described (*10-12*). Sonic disruption of *E. coli* cells was carried out with a 550 sonic dismembrator from Fisher Scientific (Pittsburgh, PA) in combination with a horn containing a ½ in. tip.

Enzymes were prepared in the same manner as previously described (*6*). WT and E288Q EcNadA were overproduced in *E. coli* BL21(DE3), purified anaerobically via immobilized metal affinity chromatography (IMAC), and reconstituted as previously described (*3*, *6*). Molecular

sieve chromatography of WT and E228Q EcNadA was performed using an ÄKTA (GE Healthcare, Piscataway, NJ) liquid chromatography system, which was maintained inside a Coy (Grass Lakes, MI) anaerobic chamber. A HiPrep 16/60 Sephacryl S-200 HR column (GE Healthcare) column was equilibrated in a buffer composed of 50 mM HEPES pH 7.5, 0.15 M KCl, 5 mM DTT, and 10% glycerol at a flow rate of 0.8 ml min^{-1}. Fractions containing aggregates of iron and sulfide eluted at 30 mL (void volume of the column), while EcNadA eluted at 60 mL. EcNadA was then concentrated and stored as aliquots in liquid N_2.

Spectroscopic Methods. UV-visible spectra were obtained on a Cary 50 spectrometer (Varian; Walnut Creek, CA) using the associated WinUV software package. Low-temperature X-band EPR spectroscopy was carried out in perpendicular mode on a Bruker (Billerica, MA) ESP 300 spectrometer equipped with an ER 041 MR microwave bridge and an ST4102 X-band resonator (Bruker). The sample temperature was maintained with an ITC503S temperature controller and an ESR900 liquid helium cryostat (Oxford Instruments; Concord, MA). Q-band EPR and ENDOR spectroscopies were performed as described previously (*13*). Mims ENDOR was performed as described (*14*, *15*).

Synthesis of 2-^{13}C DHAP. Glycerol was dissolved in water and the resulting solution was sterilized using 0.22 µm sterile filter. The reaction contained the following components in a total volume of 500 mL: 50 mM Tris-HCl, pH 8.0, 50 mM ATP, 2 mM Mg_2Cl, 20 mM β-mercaptoethanol, 0.01 mM FAD, 0.8 mM PEP, and 0.4 mM glycerol. Pyruvate kinase (26 U), glycerol-3-phosphate oxidase (6.1 U), catalase (8500 U), and glycerol kinase (3.4 U) were combined and exchanged into 50 mM Tris-HCl by gel-filtration chromatography (NICK) to remove any glycerol present in their storage buffers before they were added to the reaction mixture. The reaction was stirred at 4 °C in an open vessel and the production of DHAP was monitored spectrophotometrically in an assay containing α-glycerophosphate dehydrogenase and NADH by a decrease in absorbance at 340 nm. After determination that the reaction had

progressed at least to 95 % completion it was terminated by the addition of 2.5 L of chilled 0.16 mM HCl and then loaded onto an anion exchange column (BioRad AG1-X2, 2.5 cm × 20 cm), that was pre-equilibrated in 0.16 mM HCl at 4 °C. The column was eluted with a 1 × 1 L gradient of 0.16 mM HCl to 50 mM HCl while collecting 5 mL fractions. Fractions were assayed for DHAP as described above, and the presence of contaminating nucleotides was monitored by UV-visible absorbance at 260 nm. Fractions containing DHAP but no nucleotide contaminants were combined in a flask, and the solution was neutralized (pH ~7). The resulting solution was lyophilized to dryness by rotary evaporation and the resulting product was dissolved in a minimal volume of D_2O for NMR analysis. The contents of the NMR tube were dried again and the product was dissolved in anaerobic 50 mM HEPES, pH 7.5, in the Coy anaerobic chamber. The solution concentration was determined by the α-glycerophosphate dehydrogenase assay and stored in small aliquots in liquid N_2. Activity of synthesized DHAP was tested under anaerobic turnover conditions with WT RCN EcNadA. The purity and molecular weight were verified by ^{1}H and ^{13}C NMR and LC-MS.

Preparation of EPR samples. In 200 mM HEPES, pH 7.5, WT RCN EcNadA (1 mM) or RCN E228Q (1.5 mM) was treated with a 5-fold excess of sodium dithionite and incubated at room temperature for 5 min. The solution was placed into the EPR tube (2 mm i.d.) and frozen in isopentane chilled in liquid N_2. Samples containing IA, OAA, and/or DHAP were reduced with dithionite as described above. After the incubation period, the substrate(s) was/were added to the sample and loaded into the EPR tube and frozen in isopentane.

Preparation of ENDOR samples reduced with dithionite. In 200 mM HEPES, pH 7.5 WT RCN EcNadA (1 mM) and RCN E228Q EcNadA (1.5 mM) was treated with 5-fold excess of dithionite and incubated at room temperature for 5 min. Substrates were added to the sample, and the samples were immediately placed in Q-band EPR tubes (1 mm i.d.) and frozen in isopentane

chilled in liquid N_2. Samples with DHAP contained 15 mM DHAP or 2-^{13}C DHAP, and IA was generated via Schiff's base formation between 10 mM OAA and 0.1 M NH_4Cl or ^{15}N-NH_4Cl.

Preparation of ENDOR samples reduced by cryoreduction. In 200 mM HEPES, pH 7.5 WT RCN EcNadA (1 mM) and RCN E228Q (1.5 mM) were combined with substrate(s) as described above, and the samples were immediately placed in Q-band EPR tubes (1 mm i.d.) and frozen in isopentane chilled in liquid N_2. Samples were irradiated at 77 K in the γ-irradiation facility of the Breazeale Nuclear Reactor at the Pennsylvania State University using a ^{60}Co source (35 krad/h); a total dose of 40 kilogray was applied.

3.3 Results

Synthesis of DHAP. To synthesize DHAP selectively labeled with ^{13}C, an enzyme-catalyzed reaction was used to phosphorylate and then oxidize isotopically-labeled glycerol (Figure 3-4). Glycerol kinase was used to phosphorylate glycerol at C1 with ATP as the phosphate donor. The byproduct of this reaction, ADP was converted to ATP by the action of pyruvate kinase with phosphenolpyruvic acid (PEP). L-Glycerol-3-phosphate oxidase preferentially oxidizes C2 of glycerol-3-phosphate to form DHAP. This FAD-containing enzyme requires molecular oxygen as a cosubstrate, and catalase was added to eliminate any hydrogen peroxide. The addition of pyruvate kinase and catalase pulled the reaction to favor the product, DHAP. The formation of DHAP was monitored by the oxidation of NADH by α-glycerophosphate dehydrogenase.

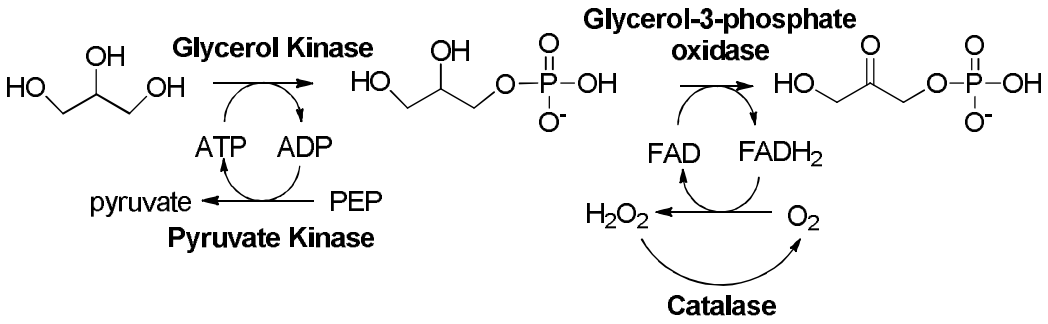

Figure **3-4**: Enzymatic reaction scheme for the production of DHAP from glycerol.

Isolation of DHAP was performed by small molecule anion exchange chromatography where separation of di- and tri- phosphates was monitored by absorbance at 260 nm. Fractions without contaminating nucleotides were assayed for DHAP by the α-glycerophosphate dehydrogenase assay and were combined and dried. Characterization of the synthesized DHAP by LC-MS showed that 97.2 % of the product was ^{13}C-DHAP. This substrate supported production of QA via NadA at a rate that was equivalent to that of commercially available DHAP.

EPR and ENDOR spectroscopy of EcNadA with DHAP. Because the ^{31}P isotope of phosphorous exhibits a nuclear spin I = ½ and has a natural abundance of 100 %, samples for ENDOR spectroscopy designed to look at phosphorous coordination to the [4Fe-4S] cluster could be prepared with commercially available DHAP. A signal arising from ^{31}P would confirm a phosphate-type ligand bound to the unique Fe site of the cluster. From previous studies, the EPR signal of WT and E228Q EcNadA in the presence of DHAP is not perturbed from that exhibited by enzyme with no substrates present, though this does not rule out an interaction between the electron spin of the Fe/S cluster and the nuclear spin of the phosphorus atom of the phosphate group (*3*). The Mims ENDOR of WT *E. coli* NadA in the presence of excess DHAP produced no

resonance in the region that a ^{31}P signal should appear (19-22 MHz) (Figure 3-5). The WT and E228Q samples containing DHAP had no resonance in this region to support a ^{31}P-Fe/S cluster interaction.

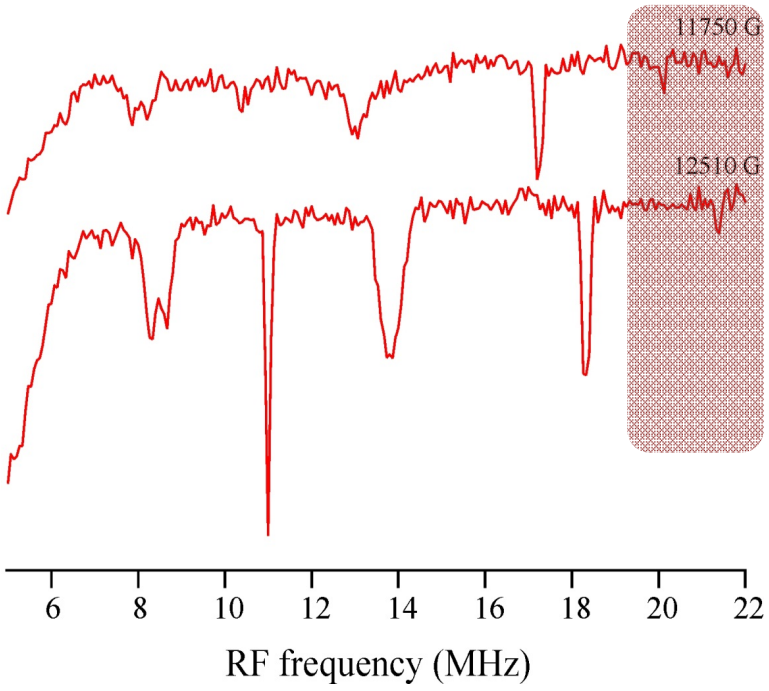

Figure **3-5**: Mims ENDOR of WT EcNadA, dithionite reduced in the presence of DHAP and OAA. Highlighted region indicates missing ^{31}P signal.

DHAP was synthesized to contain ^{13}C at C2. This labeled carbon is incorporated into QA as C5 during the NadA reaction. If the C2 oxygen of DHAP binds to the Fe/S cluster in the ground state as it is expected to bind during the dehydration of the pre-QA intermediate, the nuclear spin of C2 (^{13}C, I = ½) would be expected to perturb the electron spin of the Fe/S cluster. While this experiment monitored the interaction through two bonds, the electron and nuclear spins are expected to couple if DHAP is bound in the predicted orientation. The Mims ENDOR spectrum of WT EcNadA in the presence of 2-^{13}C DHAP showed a signal deriving from a ^{13}C

signal, yet this signal was weak and only seen in samples with OAA and NH_4Cl (Figure 3-6). Upon further examination, a natural abundance ^{13}C signal could be seen in all samples containing OAA, regardless of the presence of DHAP (Figure 3-7).

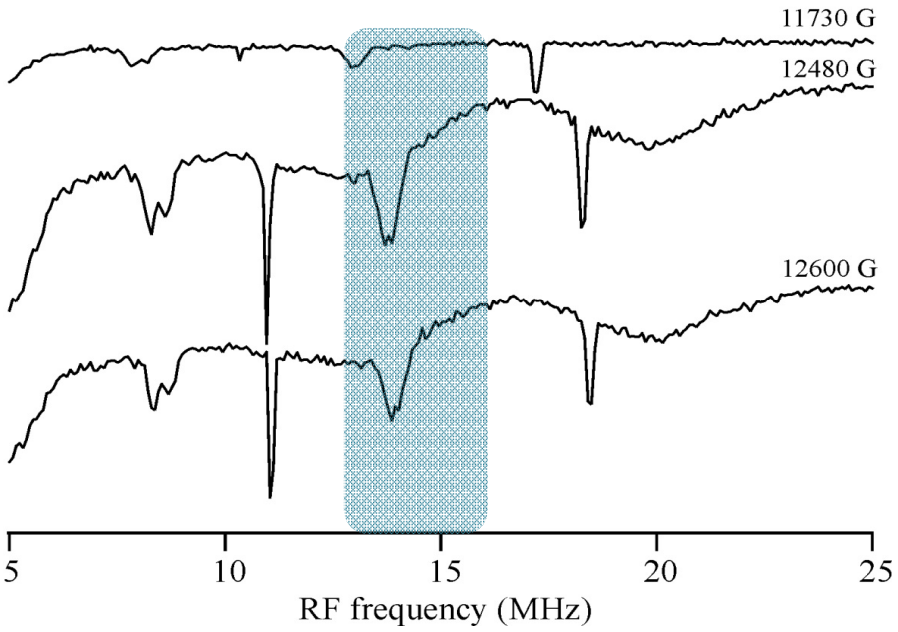

Figure **3-6**: Mims ENDOR of EcNadA WT, dithionite reduced in the presence of 2-^{13}C DHAP and IA. Highlighted region shows ^{13}C signal.

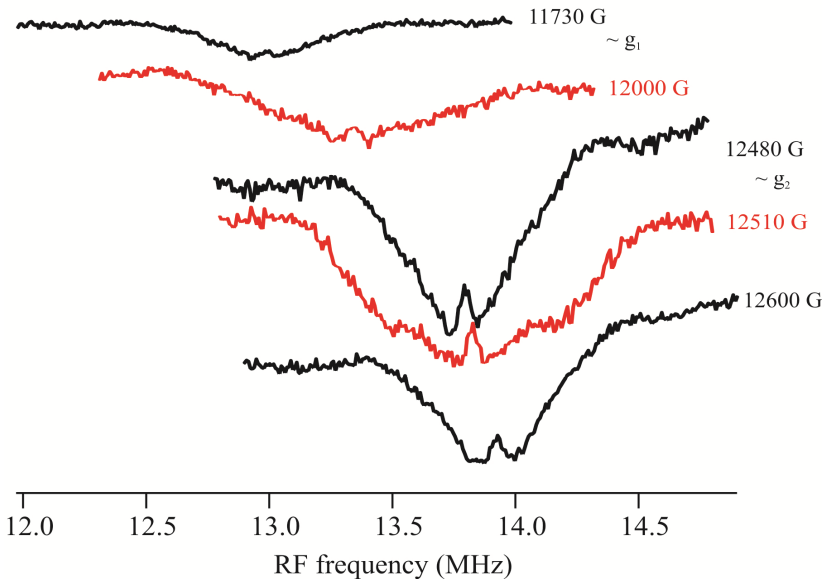

Figure **3-7**: Mims ^{13}C ENDOR of WT EcNadA. Dithionite reduced WT EcNadA in the presence of 2-^{13}C DHAP and IA (black). Dithionite reduced WT EcNadA in the presence of DHAP and IA (red).

The ENDOR samples containing DHAP or 2-^{13}C DHAP were reduced with either dithionite or γ-radiation. Since the Fe/S cluster of NadA is not typically reduced under turnover conditions, two techniques were attempted to examine whether one type of reduction led to an increase in signal. Gamma radiation produced much more intense signal at g = 2.0 indicating more organic radical species, yet both types of reduction resulted in a strong reduced species that was suitable for ENDOR spectroscopy.

While the DHAP-containing samples did not yield strong evidence that the substrate is closely or tightly bound to the Fe/S cluster, the results suggested that further investigation of the other substrate, namely IA, may identify the nature of the substrate ligand to the Fe/S cluster. Since IA can be created via OAA and an ammonium source, $^{15}NH_4Cl$ was used to create ^{15}N-IA and both EPR and ENDOR samples were made with this substrate. In duplicate samples

containing ^{15}N-IA and non-isotopically labeled IA, no ^{15}N resonance was observed in samples containing WT and E228Q EcNadA (Figure 3-8).

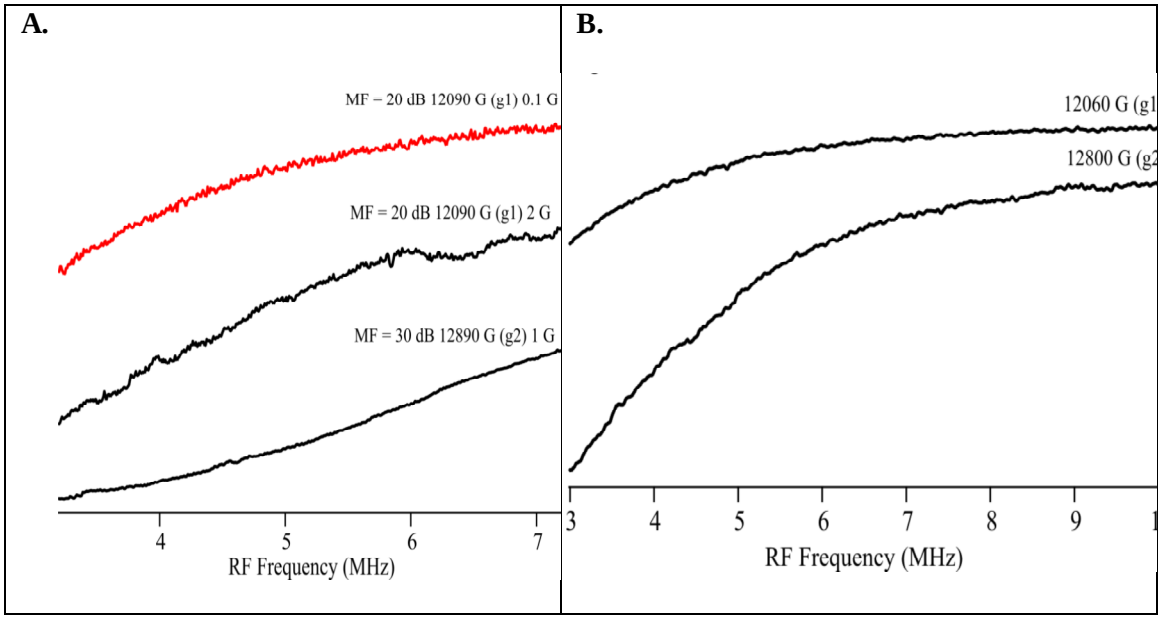

Figure **3-8**: Mims ENDOR spectra of EcNadA with $^{15}NH_4Cl$. Mims ENDOR spectrum of WT EcNadA in the presence of ^{15}N-IA (Panel A). Mims ENDOR spectrum of E228Q EcNadA in the presence of ^{15}N-IA (Panel B).

Using ENDOR as a mechanistic probe to determine the coordination at the unique Fe site in the Fe/S cluster did not resolve the type of ligand bound. Because the results of the ENDOR spectroscopic analysis seemed to contradict the previously obtained EPR analysis, the changes in the EPR spectroscopy by incubation with different substrates were re-examined. Attempts to show the same type of axial signal upon IA-binding to E228Q EcNadA was successful; however the EcNadA without substrate-bound was not as broad as observed by Saunders (*3*). This makes the difference in signal between IA absent and IA bound more subtle (Figure 3-9). The samples were prepared in the same fashion as Saunders, yet slight differences in enzyme preparation may account for spectral change. This type of tighter signal was also seen in the C294A variant used

to study the disulfide bond in EcNadA (*16*). This suggests the tighter signal may be related to the active site conformation.

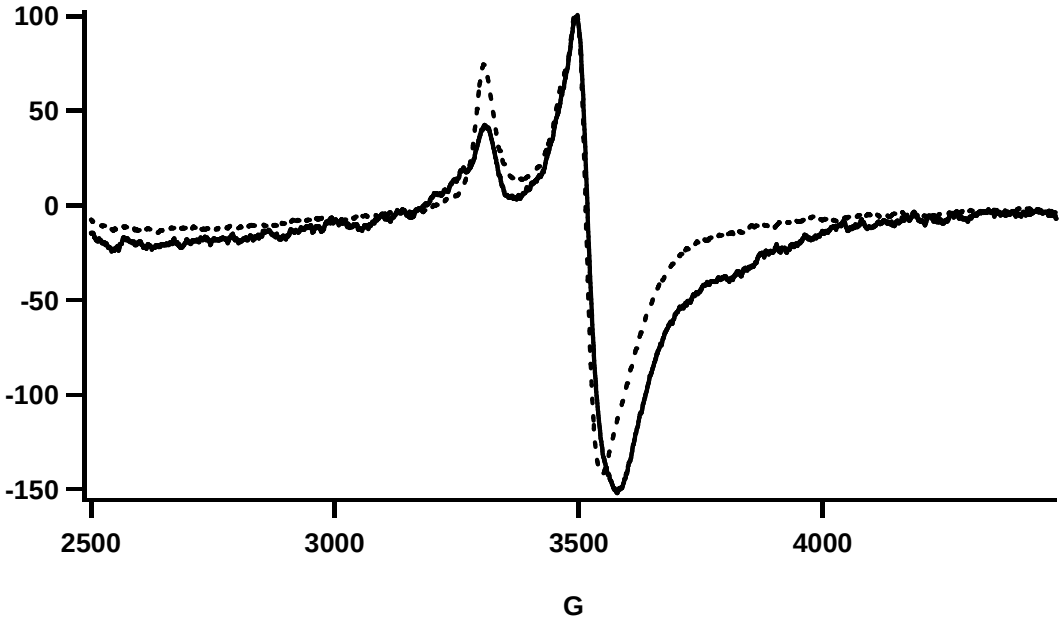

Figure **3-9**: X- band EPR of E228Q EcNadA (solid) in the presence of IA (dashed).

3.4 Discussion

It has been assumed the [4Fe-4S] cluster of NadA acts as a Lewis acid to aid in the final dehydration step of QA catalysis. The powerful spectroscopic method, ENDOR, can be utilized to determine which substrate or intermediate directly coordinates to the Fe/S cluster. This spectroscopy couples the paramagnetic $[4Fe\text{-}4S]^{+}$ cluster to a nuclear spin in the substrate. The sample is subjected to two frequencies, one corresponding to the paramagnetic center and another corresponding to the nuclear spin of the substrate. This gives rise to more intense signals, as it reports an NMR spectrum of the nuclear spin species in the vicinity of the paramagnetic center.

There are 3 possible conformations of substrates/intermediates that could bind to the Fe/S cluster. An ENDOR spectrum produced from DHAP with natural abundance ^{31}P will indicate if the phosphate group is bound through a terminal oxygen to the cluster. In both mechanisms, phosphate release is an important step in the catalytic mechanism of NadA. The Fe/S cluster could coordinate the phosphate group of the substrate DHAP to allow easier release of the moiety during catalysis. Though the phosphate group is already poised as a good leaving group, given that C1 of DHAP is electrophilic due to the adjacent carbonyl group, the Fe/S cluster may help to coordinate or anchor the substrate in the active site. In the ENDOR samples containing DHAP, no ^{31}P resonance was detected indicating the cluster is not bound to the phosphate group.

The possibility that the Fe/S cluster aids in the final dehydration was examined via ENDOR studies with 2-^{13}C DHAP. This labeled position of DHAP corresponds to C5 of QA which contains the final hydroxyl group to undergo elimination. Though the labeled position of DHAP is the carbon and not the coordinated oxygen, the coupling between the reduced Fe/S cluster and nuclear spin of the ^{13}C atom is expected to produce a detectable ENDOR signal. It was found that only a natural abundance ^{13}C signal was observed. The natural abundance ^{13}C signal was only seen in samples containing OAA. This observation suggests that either OAA binds to the Fe/S cluster, or binding of OAA produces a conformational shift of the protein and that the resulting signal is from the carbon backbone of the protein.

The failure of 2-^{13}C DHAP to produce a strong ^{13}C signal conflicts with evidence from Chan *et al*. that the Fe/S cluster does assist in the final dehydration to form QA. One possibility is that DHAP may not bind in the same orientation as the pyridine intermediates that form as catalysis proceeds. The 6-membered carbon backbone of QA in the active site may facilitate binding of the C5 hydroxyl group.

The 2-^{13}C DHAP data originally suggested IA may coordinate closer to the Fe/S cluster than DHAP. This was investigated by the presence of $^{15}NH_4Cl$ to produce ^{15}N-IA. IA was formed *in*

situ via Schiff's base formation between OAA and NH_4Cl, which were added in excess to ensure a high proportion of IA-bound enzyme. The Mims ENDOR spectra from these samples did not show evidence of coupling to any ^{15}N nucleus. While it is plausible that IA binds the Fe/S cluster via amino and carboxylate groups, as is observed in radical SAM enzymes, there is no mechanistic or structural evidence to supports this proposal. Lack of ^{15}N coupling may be due to NadA binding OAA rather than IA. As mentioned previously, the K_D for the NadA substrates is not well known and binding of the substrate may be a factor as well.

Mössbauer spectroscopy analysis performed by Chan *et al.* clearly shows that the unique iron site was bound to a product analog with two thiol groups (*8*). This bidentate binding clearly differentiated the unique iron from the other three irons of the Fe/S cluster. Since this analog is mechanistically irrelevant and contains functional groups not found in the substrate, efforts to isolate a hydroxylated QA analog in the active site would prove to be more informative.

3.5 References

(1) Nasu, S.; Wicks, D.; Gholson, R. K. L-Aspartate Oxidase, a Newly Discovered Enzyme of *Escherichia coli*, Is the B protein of Quinolinate Synthetase. *J. Biol. Chem.* **1982**, *257*, 626–632.

(2) Begley, Tadhg P., Kinsland, Cynthia, Mehl, R. A., Osterman A., Dorrestein, P. The biosynthesis of nicotinamide adenine dinucleotides in bacteria. In *Vitamins & Hormones*; 2001; pp. 103–119.

(3) Saunders, A. H. Investigation of the Structure, Function, and Regulation of Quinolinate Synthase: The Iron-Sulfur Cluster Enzyme Involved in Prokaryotic NAD Biosynthesis, The Pennsylvania State University, 2011.

(4) Cicchillo, R. M.; Tu, L.; Stromberg, J. A.; Hoffart, L. M.; Krebs, C.; Booker, S. J. *Escherichia coli* quinolinate synthetase does indeed harbor a [4Fe-4S] cluster. *Journal of the American Chemical Society* **2005**, *127*, 7310–7311.

(5) Ollagnier-de Choudens, S.; Loiseau, L.; Sanakis, Y.; Barras, F.; Fontecave, M. Quinolinate synthetase, an iron-sulfur enzyme in NAD biosynthesis. *FEBS letters* **2005**, *579*, 3737–3743.

(6) Saunders, A. H.; Griffiths, A. E.; Lee, K.-H.; Cicchillo, R. M.; Tu, L.; Stromberg, J. A.; Krebs, C.; Booker, S. J. Characterization of quinolinate synthases from *Escherichia coli*, *Mycobacterium tuberculosis*, and *Pyrococcus horikoshii* indicates that [4Fe-4S] clusters are common cofactors throughout this class of enzymes. *Biochemistry* **2008**, *47*, 10999–11012.

(7) Rousset, C.; Fontecave, M.; Ollagnier de Choudens, S. The [4Fe-4S] cluster of quinolinate synthase from *Escherichia coli*: investigation of cluster ligands. *FEBS letters* **2008**, *582*, 2937–2944.

(8) Chan, A.; Clémancey, M.; Mouesca, J.-M.; Amara, P.; Hamelin, O.; Latour, J.-M.; Ollagnier de Choudens, S. Studies of Inhibitor Binding to the [4Fe-4S] Cluster of Quinolinate Synthase. *Angewandte Chemie* **2012**, *124*, 7831–7834.

(9) Flint, D. H.; Allen, R. M. Iron-Sulfur Proteins with Nonredox Functions. *Chemical Reviews* **1996**, *7*, 2315–2334.

(10) Beinert, H. Micro Methods for the Quantitative Determination of Iron and Copper in Biological Material. *Methods Enzymol* **1978**, *54*, 435–445.

(11) Beinert, H. Semi-micro methods for analysis of labile sulfide and of labile sulfide plus sulfane sulfur in unusually stable iron-sulfur proteins. *Analytical biochemistry* **1983**, *131*, 373–378.

(12) Kennedy, M. C.; Kent, T. A.; Emptage, M.; Merkle, H.; Beinert, H.; Münck, E. Evidence for the formation of a linear [3Fe-4S] cluster in partially unfolded aconitase. *The Journal of biological chemistry* **1984**, *259*, 14463–14471.

(13) Davoust, C. E.; Doan, P. E.; Hoffman, B. M. Q-Band Pulsed Electron Spin-Echo Spectrometer and Its Application to ENDOR and ESEEM. *Journal of Magnetic Resonance* **1996**, *119*, 38–44.

(14) Mims, W. B. Pulsed Endor Experiments. *Proceedings of the Royal Society A: Mathematical, Physical and Engineering Sciences* **1965**, *283*, 452–457.

(15) Mims, W. B. Electron Paramagnetic Resonance. In *Electron Paramagnetic Resonance*; Geschwind, S., Ed.; Plenum Press: New York, 1972.

(16) Saunders, A. H.; Booker, S. J. Regulation of the Activity of *Escherichia coli* Quinolinate Synthase by Reversible Disulfide-Bond Formation. *Biochemistry* **2008**, *47*, 8467–8469.

Appendix

Site-directed mutagenesis of active site residues and kinetic studies of anSMEcpe

A.1 Introduction

Enzymes that initiate radical chemistry using *S*-adenosyl-L-methionine (SAM) are involved in thousands of reactions in all domains of life. In the radical-SAM (RS) superfamily of enzymes, SAM coordinates to a unique iron site in a [4Fe-4S] cluster, in which three of the iron ions are ligated by three cysteines found in a characteristic **C**X_3**C**X_2**C** motif. The unligated iron site allows SAM to bind in a bidentate fashion via its α-amino and α-carboxylate groups, conferring the proper orientation for radical chemistry to occur (*1*). When the [4Fe-4S] cluster is reduced to the +1 state, reductive cleavage of SAM occurs by splitting the carbon-sulfonium bond to form a 5′-deoxyadenosyl 5′-radical (5′-dA·) and L-methionine. The potent 5′-dA· can then abstract a hydrogen atom from a substrate to initiate the substrate transformation, forming 5′-deoxyadenosine (5′-dA).

RS enzymes catalyze a wide variety of reaction types, including sulfur insertion, isomerization, methylthiotransfer, and complex fragmentations and rearrangemnts; however there are only two examples of RS enzymes performing oxidative dehydrogenations (*2*). One such enzyme from *Bacillus circulans*, BtrN, oxidizes a secondary alcohol of 2-deoxy-*scyllo*-inosamine (DOIA), an intermediate in the biosynthesis of butirosin, an aminoglycoside antibiotic (*3*). This oxidation uses the 5′-dA· to abstract the hydrogen atom on C3, with ketone formation following transfer of an additional electron to a yet unknown acceptor. Comprehensive characterization of BtrN shows it contains two [4Fe-4S] clusters, where one cluster was responsible for cleaving

SAM for radical chemistry (*4*). The other cluster has been hypothesized to facilitate transfer of an electron, a product of the two-electron oxidation from an anionic radical species, back to the RS cluster for subsequent rounds of turnover (*5*). This enzyme is an example of a novel oxidation using RS chemistry, as opposed to flavin- or NAD- dependent oxidations, as well as the use of a [4Fe-4S] cluster to mediate the transfer of an electron produced from the reaction, back to the RS [4Fe-4S] cluster.

A group of RS enzymes which performs an oxidation of a substrate cysteinyl or seryl residue to generate a C_α-formylglycine (FGly) moiety are called anaerobic sulfatase maturating enzymes (anSME) (*6*). These RS dehydrogenases are unique to select prokaryotes; whereas an aerobic pathway to oxidize solely cysteinyl residues is found in eukaryotes and some prokaryotes (*7*). anSMEs act upon arylsulfatases, which hydrolyze sulfate-containing metabolites, to generate a novel formylglycine cofactor that is required for catalysis (Figure A-1). In bacteria, sulfatases are used under sulfur-starvation conditions, while eukaryotes use sulfatases to break sulfate ester linkages of metabolites. The active form of the sulfatase is the hydrated gem-diol of the formylglycyl residue, where one of the hydroxyl groups performs a nucleophilic attack on the sulfur-containing substrate to release the corresponding alcohol product. The sulfate group of the resulting enzyme-sulfate-intermediate is removed via an internal elimination process to reform the FGly residue (*8*).

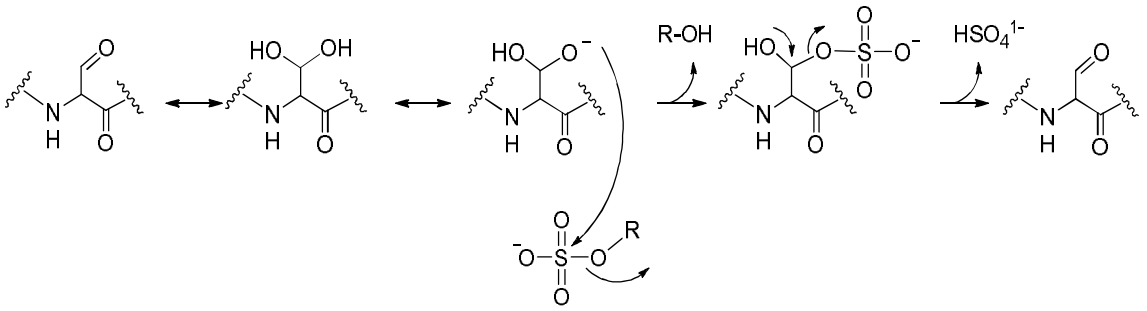

Figure **A-1:** General reaction mechanism of sulfatases.

The first well-studied case in this class of enzymes, AtsB, is an anSME from *Klebsiella pneumoniae* which contains three [4Fe-4S] clusters as shown by Mössbauer spectroscopy and quantitative iron and sulfur analyses (*9*). The native substrate, AtsA, contains an active site serine, rather than a cysteine; however, AtsB can perform the FGly transformation on either of the two residues *in vitro* (*10*). The reaction mechanism for oxidation of a cysteinyl or seryl residue is identical, with either the substrate cysteinyl or seryl residue being deprotonated as the first step of the reaction (Figure A-2). The 5′-dA· abstracts the C_β hydrogen atom from the target residue, and with loss of an additional electron to an acceptor the substrate becomes two-electron oxidized to the aldehyde (serine) or thioaldehyde (cysteine) products. The thioaldehyde is readily hydrolyzed to release hydrogen sulfide and the FGly modification. Analogous to BtrN, one round of catalysis produces an unused electron. More recently characterized is an anSME from *Clostridium perfringens* (anSMEcpe), which is an analogous protein to AtsB except its native substrate contains a cysteine. This enzyme also contains three [4Fe-4S] clusters and requires one equivalent of SAM for catalysis (*11*).

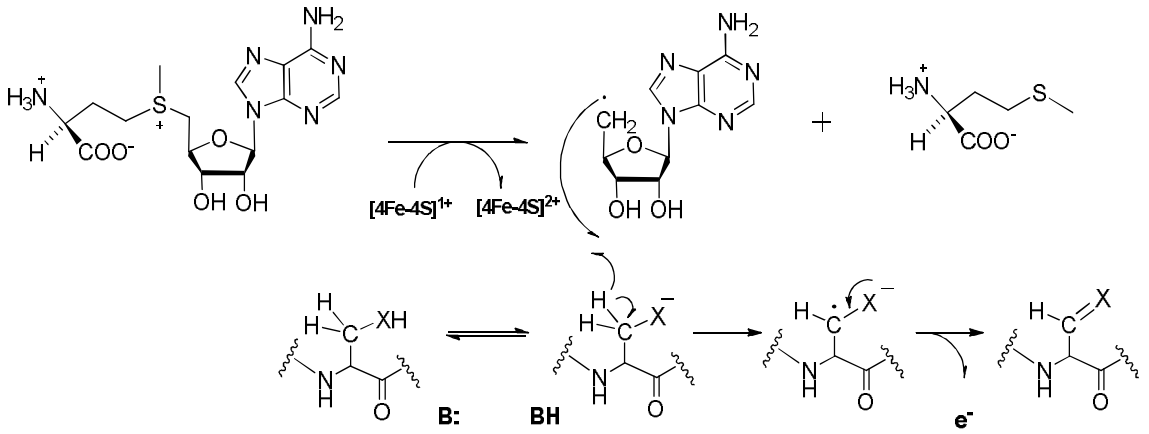

Figure **A-2**: Reaction scheme of anSME catalyzed reaction. X= O, S. If X=S, it is inferred the sulfoxide undergoes hydrolysis to form the aldehyde.

While the study of these enzymes has involved intense spectroscopic characterization, the exact mechanism of FGly formation has not been elucidated in detail (*9*). A crystal structure of anSMEcpe with a peptide substrate bound has provided greater insight into the reaction mechanism (Figure A-3) *(6)*. The location of the non-RS clusters, termed Auxiliary Cluster 1 (Aux 1) and Auxiliary Cluster 2 (Aux 2) have provided insight into how the reaction may occur. The paradigm that the Fe/S clusters shuttle the unused electron generated during each round of catalysis to an electron acceptor can be supported with this structure. One of the most notable features of the structure is the surface exposed nature of Aux 2, which may be responsible for interacting with an electron acceptor *in vivo*.

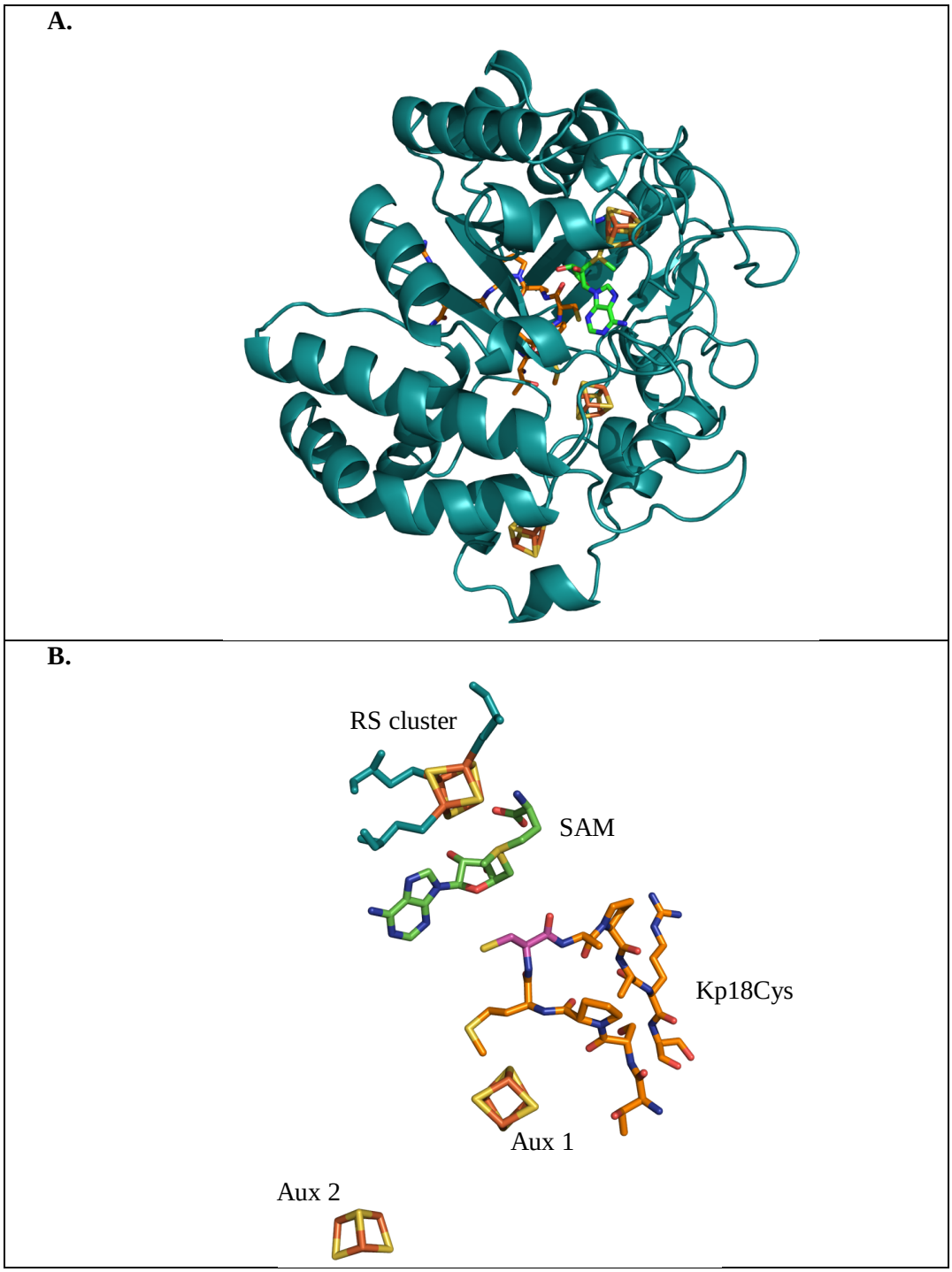

Figure **A-3**: Crystal structure of anSMEcpe. Ribbon diagram of the complete structure (Panel A). Active site with Fe/S clusters Kp9Cys (orange) with the target Cys (pink), SAM (green) (Panel B).

While the crystal structure shows a substrate peptide in the active site, previous analysis of crystals that diffracted more poorly found that the C-terminal hexahistidine tag was in the active site. The affinity tag, commonly used to quickly isolate the Fe/S cluster containing protein anaerobically in a glove box, is flexible enough to fit in the active site, suggesting the active site may accommodate peptide substrates of varying amino acid composition. Additionally, the hexahistidine tag may compete with the peptide substrate *in vitro* and may trigger unproductive cleavage of SAM.

anSME's substrate specificity has yet to be determined, as it has been with oxygen-dependent FGly generating enzymes (FGE). Determining the recognition sequence for anSMEs may allow these enzymes to be engineered into cells for *in vivo* FGly formation. The FGly moiety can be utilized as a primary functional group in bioorthogonal reactions, such that labeling of proteins can be coupled to high-yielding, easily detected products (*12*). The oxygen-dependent FGEs require the presence of proline and arginine for catalysis, yet it is unknown if these residues are absolutely necessary for catalysis in anSME.

Based on the crystal structure, two potential active site residues of anSMEcpe were changed in order to determine their activity and probe their possible role in catalysis. Further, kinetic studies with three different anSMEcpe enzyme constructs were carried out to examine if the hexahistidine tag affects catalysis by determining kinetic constants both for SAM and substrate peptide.

A.2 Materials and Methods

Materials. Oligonucleotide primers for cloning were obtained from Integrated DNA Technologies (Carlsbad, CA). PfuUltra^{TM} High Fidelity DNA Polymerase and its associated 10× reaction buffer were obtained from Stratagene (La Jolla, CA). *E. coli* strain BL21(DE3) was obtained from Novagen (Madison, WI), as were pET vectors. Coomassie blue dye-binding

reagent for protein concentration determination and the bovine serum albumin (BSA) standard (2 mg mL^{-1}) were obtained from Pierce (Rockford, IL). Nickel nitrilotriacetic acid (Ni-NTA) resin was purchased from Qiagen (Valencia, CA). Sephadex G-25 resin and PD-10, NICK and NAP pre-poured gel filtration columns were purchased from GE Biosciences (Piscataway, NJ). *S*-adenosyl-L-methionine (SAM) was synthesized enzymatically and purified as described previously (*13*). Peptides used in activity studies: Kp18Cys, Ac-NH_2-YYTSPMCAPARSMLLTGN-COOH, Kp18FGly, Ac-NH_2-YYTSPMFGlyAPARSMLLTGN-COOH; and Kp9Ser, NH_2-PMSAPARSM, were synthesized at the Penn State Molecular Biology Core Facility and purified as described (*10*). All other buffers and chemicals were of the highest grade available.

General Procedures. HPLC with detection by mass spectrometry (LC-MS) was conducted on an Agilent Technologies (Santa Clara, CA) 1200 system, which was fitted with an autosampler for sample injection and coupled to an Agilent Technologies 6410 QQQ mass spectrometer. The system was operated with the associated MassHunter software package, which was also used for data collection and analysis. Sonic disruption of *E. coli* cells was carried out with a 550 sonic dismembrator from Fisher Scientific (Pittsburgh, PA) in combination with a horn containing a ½ in. tip. Iron and sulfide analyses were carried out on AI and RCN variant proteins as previously described *(10-12)*.

Construction of N-terminal hexahistidine tagged anSMEcpe WT. pET26b anSMEcpe DNA was digested with *Nde*I and *Xho*I overnight at 37 °C and ligated into similarly digested pET28a vector by standard methods. The construct was verified by DNA-sequencing.

Construction of anSMEcpe variants. anSMEcpe variants were constructed using the QuikChange II Site-directed Mutagenesis Kit (Stratagene) according to the manufacturer's specifications, and as described previously (*14*) in which the cycling protocol is adapted for the Stratagene Robocycler thermocycler (*15*). Plasmid pET26b- anSMEcpe was used as the template

in conjunction with the appropriate primers for each respective amino acid substitution (Table A.1). All mutations were verified by DNA-sequencing of the entire gene.

Table **A.1**: Primers for site-directed mutagenesis of anSMEcpe

Forward primer for anSMEcpe Y24F	5'-GCACTTATTGTTTTTTTCATTCTTTAAGTG-3'
Reverse primer for anSMEcpe Y24F	5'-CACTTAAAGAATGAAAAAAACAATAAGTGC-3'
Forward primer for anSMEcpe D277N	5'-GGGAGTGTTTATCTTTGTAATTTTTATGTTTTAGATAAATGG-3'
Reverser primer for anSMEcpe D277N	5'-CCATTTATCTAAAACATAAAAATTACAAGGATAAACACTCCC-3'

Expression of Genes encoding anSMEcpe WT and variants. Plasmids pET26b-anSMEcpe encoding WT or variant anSMEcpe, were cotransformed into *E. coli* BL21 (DE3) with the pDB1282 plasmid as described previously (*16*). A single colony was selected to inoculate 200 mL Luria-Bertani (LB) media containing 50 µg/mL kanamycin and 100 µg/mL ampicillin and cultured overnight at 37 °C with shaking. A 160 mL portion of this culture was disturbed evenly among 6 L Erlenmeyer flasks to inoculate 16 L M9 minimal media containing 50 µg/mL kanamycin and 100 µg/mL ampicillin and the bacteria were cultured at 37 °C. At an OD_{600} = 0.3, L-(+)-arabinose and L-cysteine were added to each flask to a final concentration of 0.2 % (w/v) and 200 µM respectively. At an OD_{600} = 0.6, the flasks were placed in an ice-water bath and chilled for 20 min. IPTG and ferric chloride were added to each flask to a final concentration of 100 µM and 25 µM respectively. Cultures were incubated overnight for 16-18 hours at 18 °C. Cells were harvested by centrifugation at 6,000 × *g* for 15 min at 4 °C. The resulting cell paste was frozen in liquid N_2 and stored at - 80 °C. Typical yields were 3.1 – 3.8 g per L culture.

Purification of histagged anSMEcpe proteins. All proteins were purified in a similar fashion as that was previously described (*4*). Protein concentrations were determined by the

Bradford dye staining procedure with BSA as the standard with using a correction factor of 0.69, as previously determined (*10*). Reconstitution was carried as described (*17*) and anaerobic molecular sieve chromatography was carried out as described in Chapter 3 in 50 mM HEPES pH 7.5, 0.5 M KCl, 10 % glycerol, and 5 mM DTT.

Purification of native anSMEcpe. In a typical purification, 30 g cell paste was thawed in an anaerobic chamber in 100 mL buffer A (50 mM HEPES pH 7.5, 0.3 M KCl, 10 mM DTT). Solid egg white lysozyme was added to a final concentration of 1 mg ml^{-1}, and the solution was stirred at room temperature for 30 min. The solution was placed in an ice/water bath anend th subjected to four 1 minute bursts of sonication (setting 7). Insoluble material was removed by centrifugation at 50,000 × *g* for 1 hour at 4 °C. The resulting supernatant was placed in an ice/water bath at 0 °C, solid ammonium sulfate was added to 30 % saturation and the mixture stirred at 0 °C for 20 min. The solution was centrifuged for 30 min at 10,000 × *g* at 4 °C. The resulting supernatant was again placed in an ice/water bath at 0 °C and solid ammonium sulfate was added to 50 % saturation. After 20 min of stirring, the solution was centrifuged at 10,000 × *g* for 30 min at 4 °C. The supernatant was then discarded and the pellets were resuspended in minimal buffer B (50 mM HEPES, pH 7.5, 0.1 M KCl, 10 mM DTT). The protein was passed through a PD-10 column, pre-equilibrated in buffer B, and the collected protein was loaded onto a HiPrep Q FF 16/10 column (GE Healthcare) equilibrated in buffer B. The column was eluted with a linear gradient from buffer B to buffer C (50 mM HEPES, pH 7.5, 0.5 M KCl, 10 mM DTT) over 10 min, and 3 mL fractions were collected. Brown fractions were pooled and concentrated. The protein was then passed over a HiPrep 16/60 Sephacryl S-200 HR column (GE Healthcare), and 3 mL fractions were collected. Brown fractions were pooled and concentrated. The protein was reconstituted and subjected to gel filtration as described previously in Chapter 3.

Activity determination of anSMEcpe variants. Y24F anSMEcpe was assayed under turnover conditions in a final volume of 100 µL containing the following components: 50 mM

HEPES pH 7.5, 0.2 M KCl, 5 µM enzyme, 1 mM SAM, 500 µM Kp18Cys, and 100 µM L-tryptophan (IS). The reaction was pre-equilibrated at 37 °C for 2 min, and initiated with 2 mM dithionite. At designated times, aliquots (10 µL) of the reaction were removed and added to a solution containing 100 µM H_2SO_4 and 100 µM Kp9Ser (ES). D277N anSMEcpe was assayed in the same manner except that 100 µM enzyme was used. The quenched reaction was centrifuged at 14,000 × *g* for 30 min and analyzed by LC-MS.

Assay mixtures were separated on an Agilent Technologies Zorbax Rapid Resolution SB-C18 column (2.4 mm × 35 mm, 3.5 µm particle size), which was equilibrated in 80 % Solvent A (5 mM perfluoroheptanoic acid–6 mM ammonium formate in water, pH 3) and 20 % acetonitrile at a flow rate of 0.4 mL min^{-1}. A gradient of 20–30 % acetonitrile was applied from 0 to 2 min, and returned to 20 % acetonitrile from 2 to 2.5 min to restore the system to initial conditions. The column was allowed to re-equilibrate for 1.5 min under initial conditions before subsequent sample injections. Detection of products was performed using electrospray ionization in positive mode (ESI^+) with multiple reaction monitoring (MRM). 5′-Deoxyadenosine was detected by fragmentation of the parent ion (*m/z* = 252.1) to daughter ions of *m/z* = 136 and *m/z*= 119 with a fragmentation energy of 90 V and respective collision energies of 13 V and 50 V. Tryptophan was detected by fragmentation of the *m/z* = 188 ion with a fragmentation energy of 130 V. The resulting daughter ions, *m/z* = 146.1 and 118, were monitored with collision energies of 10 V and 21 V, respectively. To quantify the peptides, the column was equilibrated in 92 % Solvent A (0.1 % formate in water, pH 2.6) and 8 % acetonitrile at a flow rate of 0.4 mL min^{-1}. A gradient of 8–26 % acetonitrile was applied from 0.5 to 2 min, and then from 26–28 % acetonitrile from 2 to 4 min. The column was restored to initial conditions from 4 to 4.5 min and then allowed to equilibrate for another 2 min before subsequent sample injections. Detection of Kp18FGly was performed using electrospray ionization in positive mode (ESI^+) with MRM. The parent ion (*m/z*

= 1000.7) fragmented to *m/z* = 905, 404.2, and 291.4 with a fragmentation energy of 180 V. The collision energies for the fragments were 12, 20, and 24 V. Kp9Ser (ES) was monitored by fragmentation of the parent ion (*m/z* = 474.4) with fragmentation energy of 180 V, to the daughter ions (*m/z* = 719.3 and 561.3) with collision energies of 15 and 11 V, respectively.

K_M studies. The N-terminal his-tagged, C-terminal his-tagged and non his-tagged anSMEcpe proteins were assayed with various concentrations of SAM and Kp18Cys peptide to determine the K_M for each substrate. Assays contained 50 mM HEPES, pH 7.5, 0.2 M KCl, 5 µM enzyme, 500 nM SAH nucleosidase and various concentrations of SAM or Kp18Cys peptide in a final volume of 100 µL. Assays were pre-equilibrated for 3 min at 37 °C and were initiated with 1 mM dithionite. At designated times, 10 µL of the reaction mixture was quenched into 10 µL of 100 µM H_2SO_4 and 100 µM tryptophan (ES). Samples were centrifuged at 14,000 × *g* for 30 min and analyzed by LC-MS.

Assay mixtures were separated on an Agilent Technologies Zorbax Rapid Resolution SB-C18 column (4.6 mm × 50 mm, 1.8 µm particle size), which was equilibrated in 91.5 % Solvent A (0.1 % trifluoroacetic acid pH 2.6) and 9.5 % methanol at a flow rate of 0.5 mL min^{-1}. A gradient of 9.5–30 % methanol was applied from 3.3 to 4.1 min, which was followed by a gradient 30-60 % from 4.1 to 4.7 min before returning to 9.5 % methanol from 5.1 to 5.5 min to restore the system to initial conditions. The column was allowed to re-equilibrate for 2.7 min under initial conditions before subsequent sample injections. Detection of Kp18FGly and tryptophan was performed as described previously using electrospray ionization in positive mode (ESI^+) with MRM. Adenine was monitored at 0.9 min by fragmentation of *m/z* = 136.1 to *m/z* = 65.1 with a fragmentation energy of 90 V and a collision energy of 50 V.

A.3 Results

Characterization of active site anSMEcpe variants. Site-directed mutagenesis was carried out and the mutations were verified by nucleic acid sequencing. The plasmid was co-transformed into BL21 with pDB1282 and overexpressed in M9 minimal media with induction of the anSMEcpe at 18 °C for 16 hours (Figure A-4). Typical yields of cell paste were 2.8-3.4 g per L liquid culture, similar to that of WT anSMEcpe. The cells were lysed and protein purification was carried out under strict anaerobic conditions in the Coy anaerobic chamber (Figure A.4). Protein yields for D277N anSMEcpe were much lower (1.88 mg/L culture) as compared to the Y24F variant (4.88 mg/L culture). Both variant proteins, as well as WT anSMEcpe, were reconstituted to ensure maximum Fe/S content. After reconstitution, the characteristic 280/400 nm absorbance ratio decreased from 2.6 to 2.0 for the D277N variant, and 2.67 to 1.8 for the Y24F variant (Figure A-5).

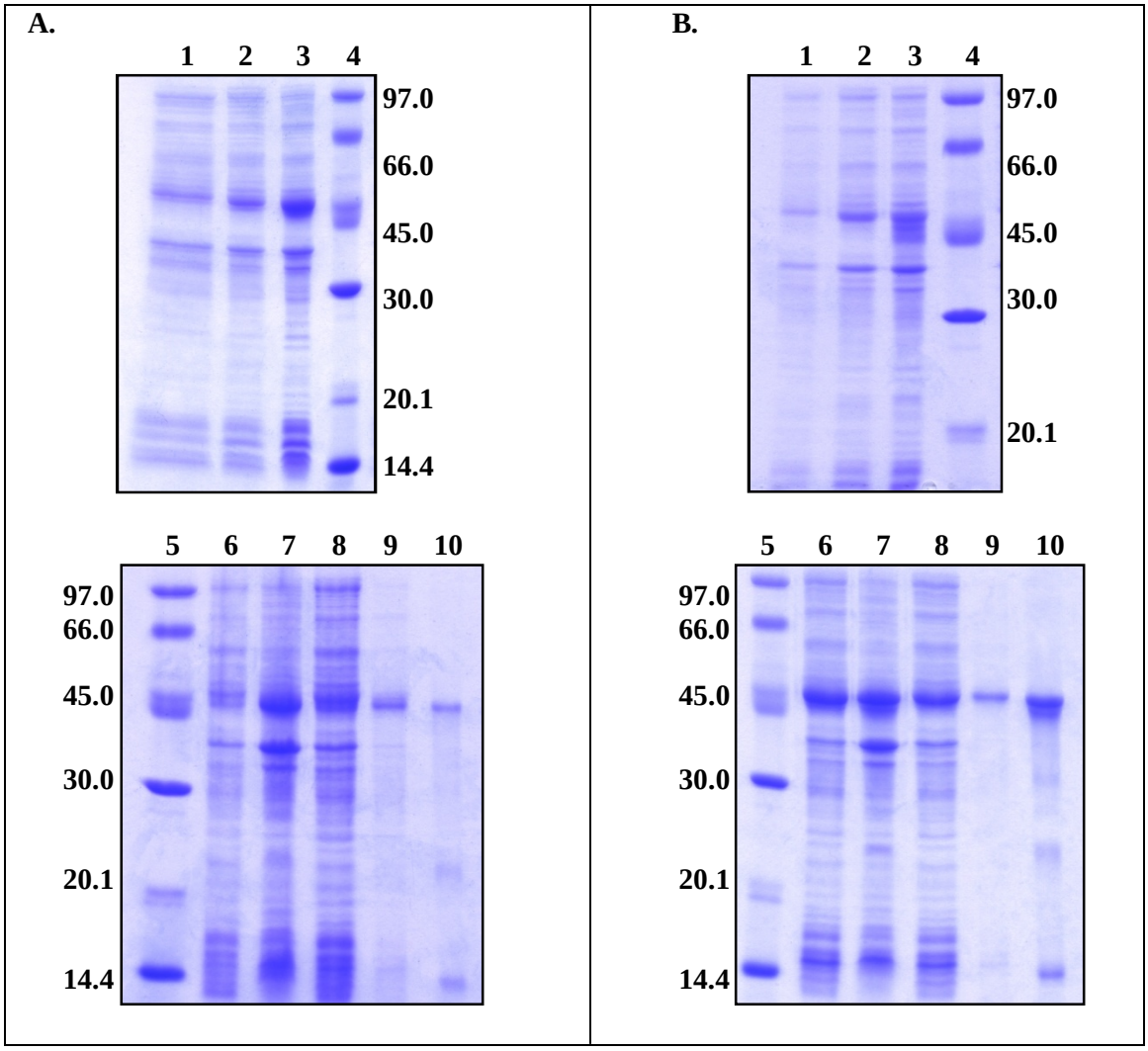

Figure **A-4**: Expression and purification SDS-PAGE of anSMEcpe variants. D277N (Panel A). Y24F (Panel B).

Lanes: **1**, molecular weight markers; **2**, prior to pDB1282 induction; **3**, prior to anSMEcpe induction, **4**; post induction, **5**, molecular weight markers; **6**, crude lysate supernatant; **7**, crude lysate pellet; **8**, Ni-NTA load eluate; **9**, Ni-NTA wash eluate; **10**, purified and concentrated protein.

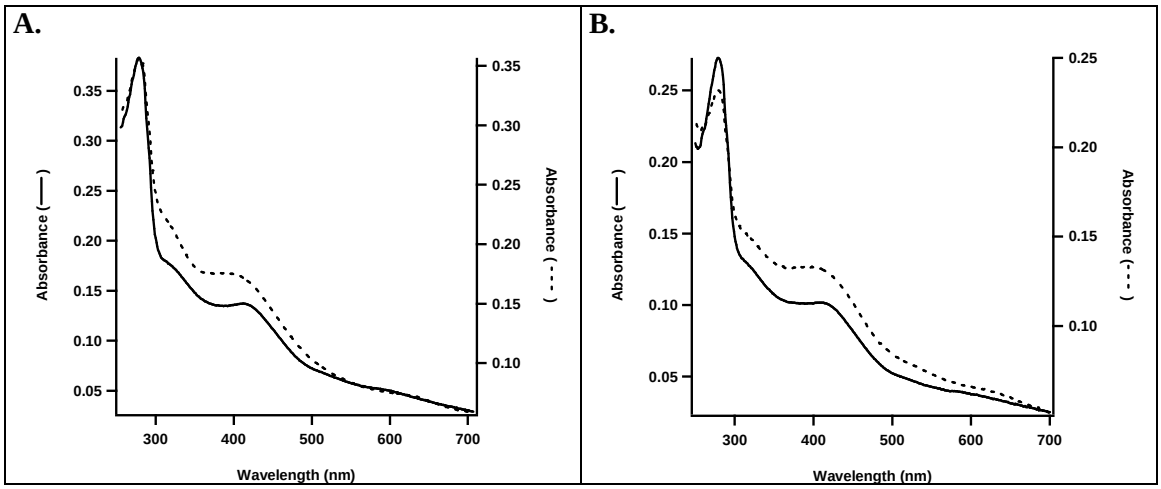

Figure **A-5**: UV-visible spectrum of anSMEcpe variants. D277N; AI (solid line) and RCN (dashed) (Panel A) Y24F; AI (solid line) RCN (dashed) (Panel B).

To determine whether these D277 and Y24 are important active site residues, the activity of the variants was determined. The aspartic acid residue, D277, was changed to an asparagine to remove an active site base. This variant protein has a $[V]/E_T$ that is 500 times slower than the wild-type enzyme in FGly formation (Figure A-6). The other variant, Y24F, had a specific activity of 65 µmol min^{-1} mg^{-1}, which is approximately four-fold lower than that of WT enzyme (263 µmol min^{-1} mg^{-1}). This residue is in close proximity to the Fe/S cluster and the sulfonium of SAM and the reduced activity when changed to phenylalanine demonstrates how the residue affects activity.

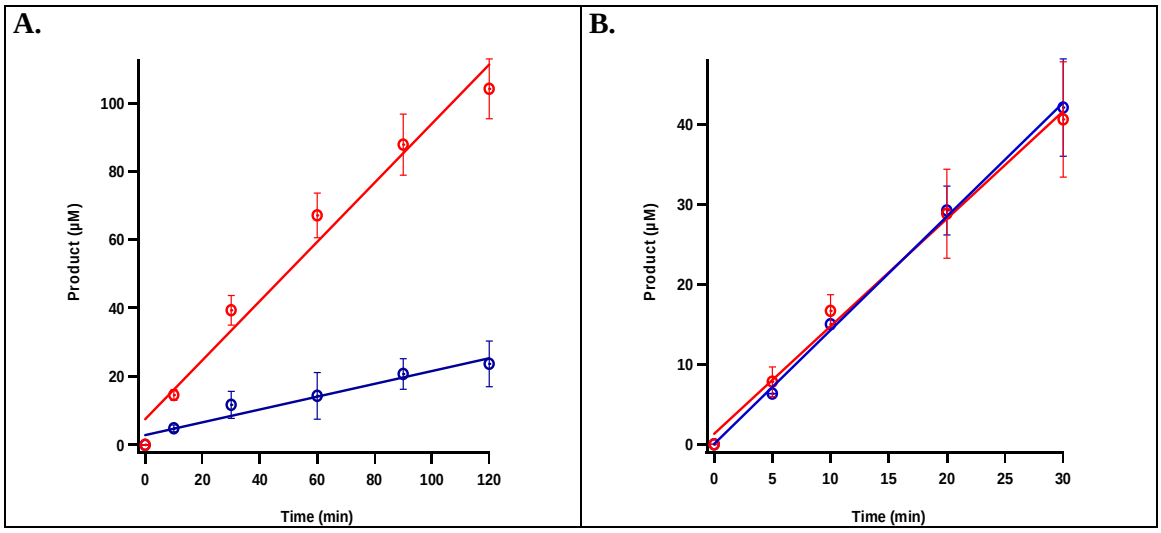

Figure **A-6**: Activity of anSMEcpe variants. D277N; FGly (blue) 5′-dA (red) (Panel A). Y24F; FGly (blue) 5′-dA (red) (Panel B).

K_M studies of WT anSMEcpe. Three different WT anSMEcpe constructs were generated by inserting the anSMEcpe gene into various plasmids. Because WT anSMEcpe was originally isolated and crystallized with the C-terminal hexahistidine tag in the active site, anSMEcpe was isolated without a hexahistidine tag and with an N-terminal hexahistidine tag, in hope that the removal of the tag or its attachment to the opposite terminus would prevent alteration of anSME activity by the tag. The N-terminal hexahistidine construct of anSMEcpe was generated by cloning the anSMEcpe into pET28a using the *Nde*I and *Xho*I restriction sites and overexpressing the protein in BL21(DE3). The protein yield was much less than that for C-terminal hexahistidine tagged anSMEcpe, and was similar to that obtained by Benjdia *et al.* (0.4 mg/L culture AI) *(7)*.

anSMEcpe lacking a hexahistidine tag was overexpressed and purified in a manner similar to that described by Goldman *et al* (*18*). The gene was cloned into a pET26b plasmid with a stop codon (TAA) inserted at the end of the gene, preventing expression of the C-terminal

hexahistidine tag. Expression of this protein was difficult to determine by SDS-PAGE with coomassie staining; however, a small amount of protein was isolated during the purification (1.2 mg/ L culture).

Hexahistidine-tagged anSMEcpe (C-terminus and N-terminus) and native anSMEcpe were subjected to reconstitution and subsequent size-exclusion chromatography to remove protein aggregates and other molecules. The resulting proteins were individually assayed with various concentrations of SAM or Kp18Cys, and initial velocities were plotted versus concentration of substrate to yield a Michaelis-Menten curve. When SAM was the varied substrate, the plots were fitted to the standard Michaelis-Menten equation (Equation 1) using IgorPro (Wavemetrics, Inc., Portland, OR) where v is the initial velocity, V_{max} is the maximum rate, S is the varied substrate concentration, and K_M is the Michaelis constant for the substrate.

$$v = \frac{V_{max}[S]}{K_M + [S]} \qquad \text{Equation 1}$$

Varying the peptide substrate showed inhibition and was therefore fit to Michaelis-Menten kinetics accounting for substrate inhibition (Equation 2), where K_I is the dissociation constant for the inhibiting substrate.

$$v = \frac{V_{max}[S]}{K_M + [S]\left(1 + \frac{[S]}{K_I}\right)} \qquad \text{Equation 2}$$

Data was obtained for both products of the reaction. 5′-Deoxyadenosine was determined as adenine via the action of SAH nucleosidase, which was added to the assay to reduce product inhibition by combined effects of 5′-dA and methionine. The K_M constants obtained from the two products are within 1-2 standard deviations of each other.

Table **A.2:** K_M for anSMEcpe with various affinity tags.

	K_M SAM (μM)		K_M Kp18Cys (μM)	
	Adenine	FGly	Adenine	FGly
N-terminal hexahistidine tag anSMEcpe	261.3 ± 98.6	437.2 ± 74.9	213.56 ± 69.7 [K_I = 2633.8 ± 970]	269 ± 88.7 [K_I = 729.25 ± 198]
C-terminal hexahistidine tag anSMEcpe	165.0 ± 41.7	255 ± 52	154.56 ± 52 [K_I = 560 ± 221]	
anSMEcpe lacking hexahistidine tag	378.1 ± 91.1	322.6 ± 49.7	69.5 ± 27.2 [K_I = 760.7 ± 299]	68.34 ± 34.2 [K_I = 302.4 ± 84.9]

A.4 Discussion

Two active site residues, D277 and Y24, are in close proximity to the active site of anSMEcpe (Figure A-7). D277 is hypothesized to deprotonate the sulfhydryl residue to form the anionic thiol moiety. This deprotonation is essential for the initation of catalysis, accounting for the severely diminished activity observed in enzymatic assays.

The methyl group on the sulfonium of SAM is directed toward Y24 (Figure A-7). This aromatic residue may act to stabilize intermediates through a π–cation interaction. When changed to a phenylalanine, the aromatic functionality still stabilizes SAM albeit not as well as tyrosine. This explains the reduced rate of turnover of the Y24F variant.

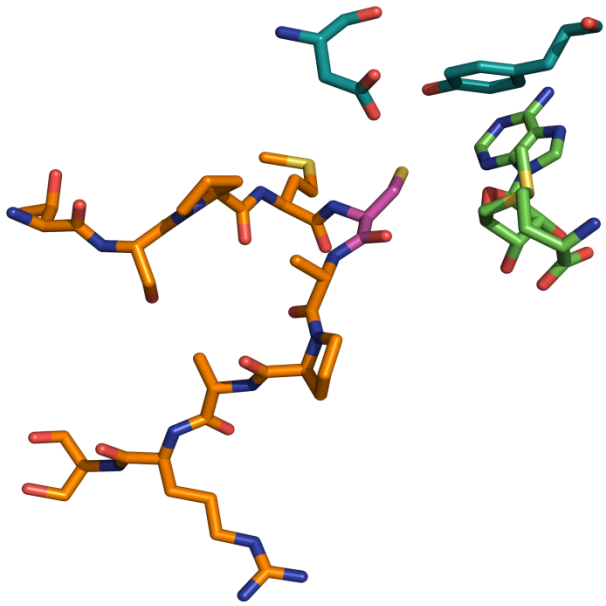

Figure **A-7**: Active site of anSMEcpe with substrate peptide and SAM bound.

Kinetic studies to show if the hexahistidine affinity tags on anSMEcpe affect catalysis were carried out by analyzing the Michaelis-Menten constants for the three different enzyme constructs. The lack of reported kinetic analyzes of RS enzymes exemplifies the complex catalytic mechanisms of most RS enzymes. The K_M constants for SAM are slightly lower than the reported K_M constant for BtrN of 460 ± 100 µM *(18)*.

The reported K_M values for the peptide substrate Kp18Cys show a much more varied response with the non histagged anSMEcpe reporting the lowest K_M values. Significant inhibition was seen as higher concentrations of peptide were used and data were more accurately fitted to equations that accounted for substrate inhibition. Future work should include assaying these enzymes with different peptide substrates containing variable amino acids to find the minimal sequence for anSMEcpe to recognize for catalysis.

A.5 References

(1) Walsby, C. J.; Ortillo, D.; Broderick, W. E.; Broderick, J. B.; Hoffman, B. M. An anchoring role for FeS clusters: chelation of the amino acid moiety of S-adenosylmethionine to the unique iron site of the [4Fe-4S] cluster of pyruvate formate-lyase activating enzyme. *Journal of the American Chemical Society* **2002**, *124*, 11270–11271.

(2) Lanz, N. D.; Booker, S. J. Identification and function of auxiliary iron-sulfur clusters in radical SAM enzymes. *Biochimica et biophysica acta* **2012**, *1824*, 1196–1212.

(3) Ruszczycky, M. W.; Ogasawara, Y.; Liu, H.-W. Radical SAM enzymes in the biosynthesis of sugar-containing natural products. *Biochimica et biophysica acta* **2011**.

(4) Grove, T. L.; Ahlum, J. H.; Sharma, P.; Krebs, C.; Booker, S. J. A consensus mechanism for Radical SAM-dependent dehydrogenation? BtrN contains two [4Fe-4S] clusters. *Biochemistry* **2010**, *49*, 3783–5.

(5) Benjdia, A.; Subramanian, S.; Leprince, J.; Vaudry, H.; Johnson, M. K.; Berteau, O. Anaerobic sulfatase-maturating enzymes, first dual substrate radical S-adenosylmethionine enzymes. *The Journal of biological chemistry* **2008**, *283*, 17815–26.

(6) Berteau, O.; Guillot, A.; Benjdia, A.; Rabot, S. A new type of bacterial sulfatase reveals a novel maturation pathway in prokaryotes. *The Journal of biological chemistry* **2006**, *281*, 22464–22470.

(7) Roeser, D., Preusser-Kunze, A., Schmidt, B., Gasow, K., Wittmann, J. G., Dierks, T., von Figura, K., and Rudolph, M. G. A general binding mechanism for all human sulfatases by the formylglycine-generating enzyme. *Proceedings of the National Academy of Sciences of the United States of America* **2006**, *103*, 86–91.

(8) Hanson, S. R.; Best, M. D.; Wong, C.-H. Sulfatases: Structure, Mechanism, Biological Activity, Inhibition, and Synthetic Utility. *Angewandte Chemie (International ed. in English)* **2004**, *43*, 5736–5763.

(9) Grove, T. L.; Lee, K.; Clair, J. S.; Krebs, C.; Booker, S. J. *In vitro* characterization of AtsB, a Radical SAM formylglycine-Generating Enzyme That contains Three [4Fe-4S] Clusters. *Biochemistry* **2008**, *47*, 7523–7538.

(10) Grove, T. L.; Ahlum, J. H.; Qin, M.; Lanz, N.; Radle, M. I.; Krebs, C.; Booker, S. J. Further Characterization of Cys-Type and Ser-Type Anaerobic Sulfatase Maturating Enzymes Suggests a Commonality in Mechanism of Catalysis **2012**.

(11) Benjdia, A.; Subramanian, S.; Leprince, J.; Vaudry, H.; Michael, K. Anaerobic Sulfatase-Maturating Enzyme : A Mechanistic Link with Glycyl Radical Activating Enzymes? *FEBS J.* **2010**, *277*, 1906–1920.

(12) Rabuka, D. Chemoenzymatic Methods for Site-Specific Protein Modification. *Curr Opin Chem Biol* **2010**, *14*, 790–796.

(13) Iwig, D. F.; Booker, S. J. Insight into the polar reactivity of the onium chalcogen analogues of S-adenosyl-L-methionine. *Biochemistry* **2004**, *43*, 13496.

(14) Cicchillo, R. M.; Lee, K.-H.; Baleanu-Gogonea, C.; Nesbitt, N. M.; Krebs, C.; Booker, S. J. *Escheriachia coli* lipoyl synthase binds two distinct [4Fe-4S] clusters per polypeptide. *Biochemistry* **2004**, *43*, 11770–11781.

(15) Ramamurthy, V.; Swann, S. L.; Paulson, J. L.; Spedaliere, C. J.; Mueller, E. G. Critical aspartic acid residues in pseudouridine synthases. *The Journal of biological chemistry* **1999**, *274*, 22225–30.

(16) Cicchillo, R. M.; Iwig, D. F.; Jones, A. D.; Nesbitt, N. M.; Baleanu-Gogonea, C.; Souder, M. G.; Tu, L.; Booker, S. J. Lipoyl synthase requires two equivalents of S-adenosyl-L-methionite to synthesize one equivalent of lipoic acid. *Biochemistry* **2004**, *43*, 6378–6386.

(17) Saunders, A. H.; Griffiths, A. E.; Lee, K.-H.; Cicchillo, R. M.; Tu, L.; Stromberg, J. A.; Krebs, C.; Booker, S. J. Characterization of quinolinate synthases from *Escherichia coli*, *Mycobacterium tuberculosis*, and *Pyrococcus horikoshii* indicates that [4Fe-4S] clusters are common cofactors throughout this class of enzymes. *Biochemistry* **2008**, *47*, 10999–11012.

(18) Goldman, P.; Grove, T. L.; Booker, S. J.; Drennan, C. Crystal Structure of anSMEcpe **2012**.